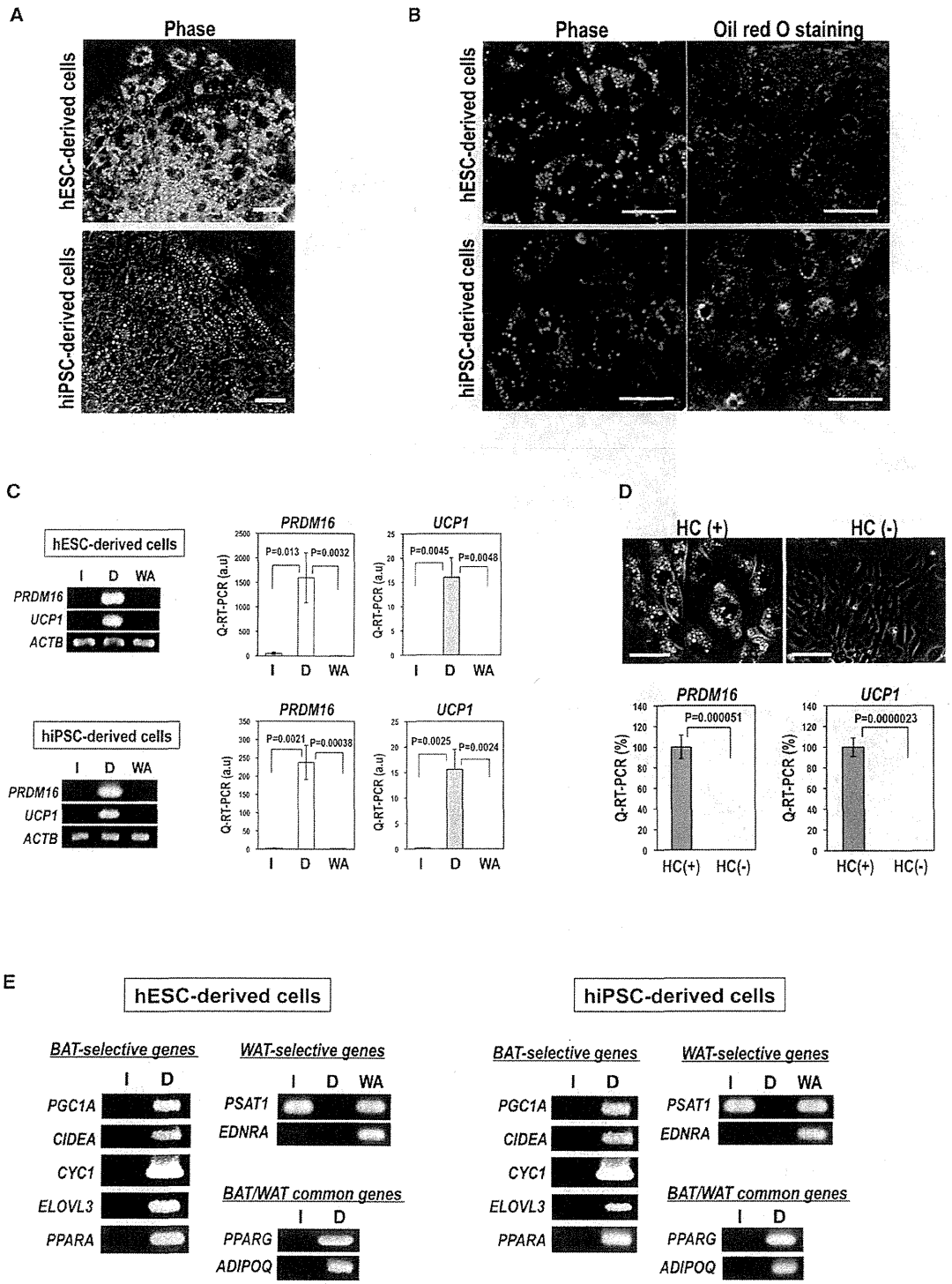

Figure 1. Differentiation of hPSCs into BAs

(A) Microscopy of hPSC-derived cells. Scale bar, 50 μm.

(B) Oil red O staining (right) with phase contrast microscopy (left). Scale bar, 40 μm.

(C) Expression of *PRDM16* and *UCP1* determined by RT-PCR (left) or real-time PCR (middle and right). The error bars represent average ± standard deviation (SD) (n = 3).

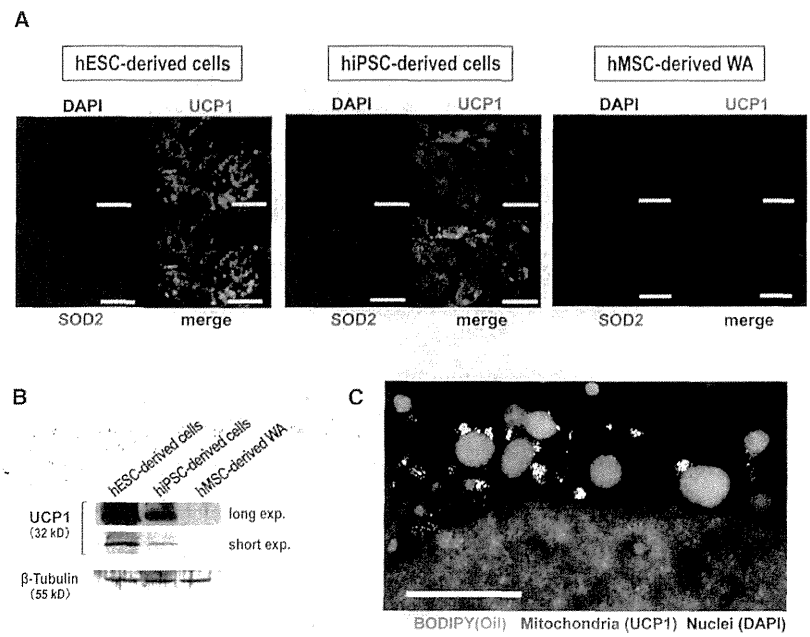

Figure 2. Analyses on Protein Expressions and Fine Structures

(A) Immunostaining using an anti-UCP1 and anti-SOD2 antibody as indicated. Scale bar, 50 μm.

(B) Western blotting using an anti-UCP1 as indicated.

(C) Lipid staining. hESC-derived differentiated cells were stained by an anti-UCP1 antibody (red) and BODIPY 493/503 (green). Scale bar, 5 μm.

(D) EM of hiPSC-derived cells (left) and hESC-derived cells (right). L, lipid droplets; M, mitochondria. Scale bar, 2 μm.

n = 3) (Figure 4D). Surprisingly, hMSCdWA-transplanted mice showed elevated homeostasis model assessment-insulin resistance (HOMA-IR) values compared not only with hESCdBA-transplanted mice ($p = 0.0003$; $n = 3$) but also with saline-injected mice ($p = 0.0011$; $n = 3$) (Figure 4E), indicating that hMSCdWA induces insulin resistance despite its favorable effect on lipid metabolism. Similar results were obtained when 6-week-old younger mice were used for the assay (data not shown). As shown in Figure 4F, oral glucose tolerance tests (OGTTs) further demonstrated that hESCdBA transplantation reduced 15 min blood glucose values compared to saline injected ($p = 0.010$; $n = 3$), while hMSCdWA-transplanted mice exhibited elevated 30 min blood glucose values compared not only with hESCdBA-transplanted mice ($p = 0.0034$; $n = 3$) but also with saline-injected mice ($p = 0.0055$; $n = 3$). Similar results were obtained when 6-week-old younger mice were used for the assay (data not shown), confirming that hMSCdWA transplantation deteriorates glucose metabolism. The different effects between hESCdBA and hMSCdWA were not due to the difference in cell survival, as we clearly detected the existence of transplanted cells (Figure S4A). Moreover, deterioration of glucose metabolism by hMSCdWA transplantation could not be attributed to inflammation, because we did not observe any signs of inflammation, such as macrophage infiltration (Figure S4B). In addition, hMSCdWA did not express tumor necrosis factor α (*TNFA*), and it expressed only a low level of *IL1B* (Figure S4C).

We also examined longer-term effects of hPSCdBA transplantation using immunocompromised NOG mice (Ito et al., 2002). Fasting blood glucose level-lowering effects of hESCdBA were determined at least for 3 weeks (Figure 4G). Cells with multilocular lipid droplet (Figure 4H) that expressed UCP1 (Figure 4I) and human HLA-A,B,C (Figure 4J) were determined by histological analyses. Around the graft tissue, microvasculatures were also detected (Figure 4H arrowheads).

Finally, we assessed possible therapeutic effect of hESCdBA on hMSCdWA-induced deterioration of glucose metabolism. Although no significant changes in fasting blood glucose values and HOMA-IR values were observed (Figure 4K and 4L), cotransplantation of an equivalent number of hESCdBA ameliorated the deleterious effect of hMSCdWA, significantly lowering the 30 min blood glucose values ($p = 0.0014$; $n = 3$) (Figure 4M).

All those findings together indicate that (1) hPSCdBAs improve both lipid and glucose metabolism, (2) hMSCdWA improved lipid but deteriorates glucose metabolism, and (3) hPSCdBAs ameliorate adverse effects of hMSCdWA on glucose metabolism.

(D) BA differentiation in the presence or absence of HC. Microscopy (upper) and expressions of *PRDM16* (lower left) and *UCP-1* (lower right) by real time PCR were shown. Scale bar, 50 μm. The error bars represent average ± SD ($n = 3$).

(E) Expression of BAT-selective, BAT/WAT-common, and WAT-selective genes examined by RT-PCR. I, immature hPSC; D, differentiated hPSC; WA, hMSCdWA.

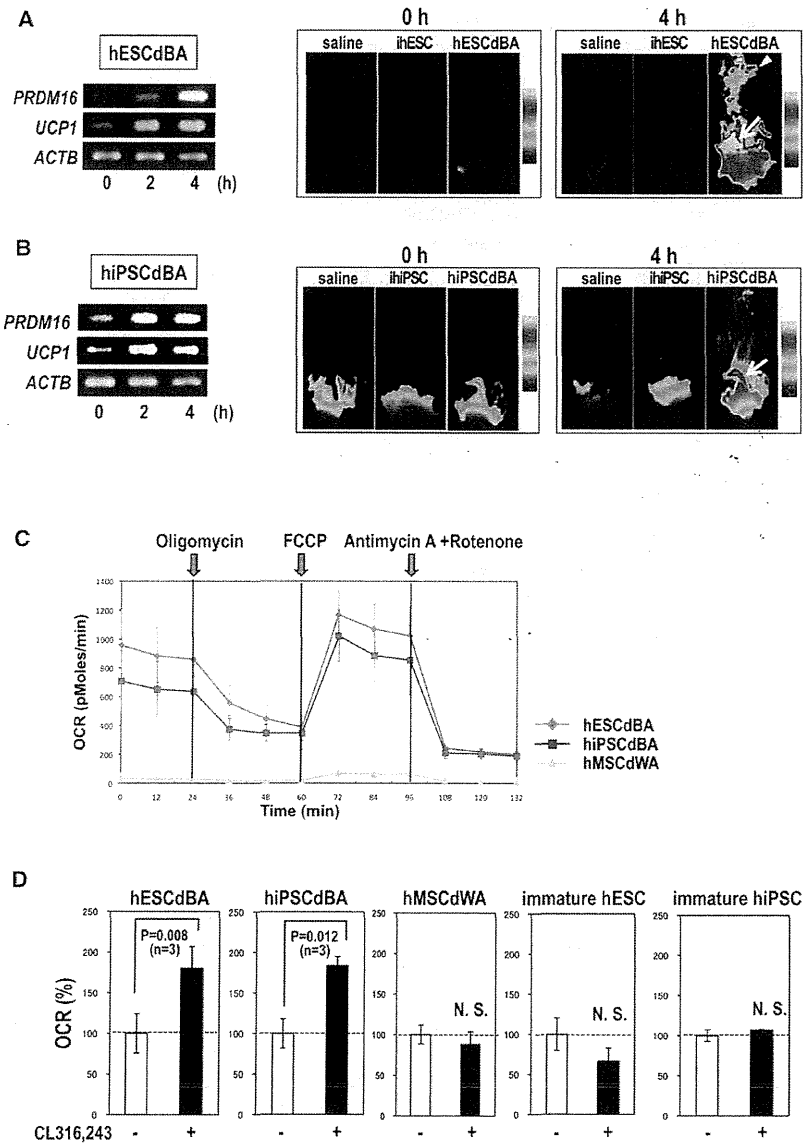

Figure 3. Thermogenic and Mitochondrial Respiratory Activation

(A and B) Thermogenesis studies. hESCdBA (A) and hiPSCdBA (B) were treated with isoproterenol. Gene expression was examined by RT-PCR over time (A, left; B, left). Thermographic images of mice transplanted with saline, immature hESC (ihESC), hESCdBA, immature hiPSC (ihiPSC), or hiPSCdBA before and after isoproterenol treatments are shown (A, right; B, right). Arrows indicate regions of transplantation; arrowheads indicate areas of endogenous murine BAT.

(C) Mito stress tests were performed using hESCdBA, hiPSCdBA, and hMSCdWA as indicated.

(D) OCR was measured in hESCdBA, hiPSCdBA, hMSCdWA, immature hESCs, and immature hiPSCs after a 4 hr incubation with or without CL316,243. The error bars in (C) and (D) represent average ± SD (n = 3).

Signaling for BA Differentiation

To confirm that our differentiation technique correctly reproduced classical BAT development via myoblastic differentiation (Timmons et al., 2007; Seale et al., 2008; Sun et al., 2011), the expression of a series of developmental markers was examined. As shown in Figure 5A, myoblastic *MYF5* expression was transiently upregulated during the initial floating culture step of differentiation. Moreover, the expression of a paraxial mesoderm marker, platelet-derived growth factor receptor α (*PDGFRA*) (Sakurai et al., 2006), was upregulated. By contrast, the levels of immature mesenchymal stem cell marker, *NG2* and *PDGFRB* (Crisan et al., 2008), as well as a lateral plate mesoderm marker, VEGFR2 (Sakurai et al., 2006), were reduced. The precedence of myoblastic differentiation was further confirmed by the transient induction of PAX3/7, which are involved in myogenic commitment (Figure 5B). Thus, our method correctly mimics the classical BAT development but not a brite adipocyte pathway via immature mesenchymal stem cell differentiation.

We further evaluated the detailed role of each hematopoietin. The absence of any one of the components of HC lowered the quality of BA differentiation, reducing cellular viability and/or percentages of multilocular lipid-containing cells (Figure 5C). Gene expression studies further showed that VEGF was required for *PRDM16* expression, whereas KITLG, IL6, or FLT3LG was required for subsequent *UCP1* expression (Figure 5D). Surprisingly, depletion of either KITLG, IL6, or FLT3LG paradoxically induced the expression of a WAT marker, phosphoserine aminotransferase 1 (*PSAT1*) (Seale et al., 2007), and a lateral plate mesoderm marker, vegfr2. Thus, the HC is essential for the differentiation of hPSCs into classical BA, and the omission of any of the HC components results in WAT lineage commitment.

We also examined intracellular signaling by performing inhibitor analyses. Because a BMPR1a inhibitor (BMPR1a-i) and p38 MAPK inhibitor (p38-i) reportedly hamper BA differentiation (Sellayah et al., 2011), effects of these two inhibitors, along with those of a MAP kinase-ERK kinase (MEK) inhibitor (MEK-i), were examined. We found that BMPR1a-i induced massive cell death during the floating culture step of BA differentiation (Figure 5E, second left). Cell death had been induced as early as day 1 (data not shown). Similar results were obtained from the case of AKT inhibitor (AKT-i). (Figure 5E, right). Thus, BMPR1a-dependent signaling is required for the survival of immature sphere-forming progenitor cells, from which mature BA will be produced. We then followed up the p38-i- and MEK-i-treated

cells until day 10, when mature BA was generated. In the case of hESC, p38-i treatment reduced the number of lipid droplet-containing cells (Figure 5F, upper middle), while MEK-i treatment exerted minimal effects (Figure 5F, upper right). Compatible to these morphological findings, p38-i treatment, but not MEK-i treatment, lowered *PRDM16* and *UCP1* expression levels (Figure 5G, left half). By contrast, p38-i treatment exerted minimal effects on hiPSCs (Figure 5F, lower middle), whereas MEK-i treatment induced cogeneration of the cells with unilocular lipid droplets (Figure 5F, lower right). Compatibly, *PRDM16* and *UCP1* expressions were only slightly reduced in p38-i-treated hiPSCs but clearly reduced in MEK-treated hiPSCs (Figure 5G, right half). Therefore, p38 MAPK and ERK signaling play important roles in BA differentiation depending on the lines or kinds of hPSCs.

A Functional Link between BA and Hematopoiesis

There has been a controversy regarding the effect of BM adipocytes on the proliferation and differentiation of committed HPCs. For example, murine BM adipocytic lines are reportedly capable of supporting lymphopoiesis (Gimble et al., 1990) and granulopoiesis (Gimble et al., 1992), whereas human BM-derived fat cells generated by a dexamethasone/insulin treatment reduce colony-forming capacities of HPCs (Ookura et al., 2007). We hypothesized that the controversy came from the heterogeneity of BM adipocytes and that BA, but not WA, serves as a stroma for committed HPCs for the following reasons: (1) hematopoietic stromal cells essential for maintaining CFU-S exhibit morphological resemblance to BA rather than to WA (Dexter et al., 1977); (2) the murine embryo-derived C3H10T1/2 cell line (Reznikoff et al., 1973), which differentiates into mature BAT on BMP7 treatment (Tseng et al., 2008), is widely used as a feeder for the hematopoietic differentiation of monkey (Hiroyama et al., 2006) and human (Takayama et al., 2008) ESCs; (3) BM is replaced by WA in severe myelosuppressive states including aplastic anemia; and (4) treatment with dexamethasone/insulin induces differentiation into WA but not BA.

To validate our hypothesis, human umbilical cord blood $CD34^+$ HPCs were cultured on hESCdBA layers for 1 week in the absence of any recombinant hematopoietic cytokines. Then, floating cells were subjected to intrabone marrow transplantation (IBM-T) into alymphocytic NOG mice, and after 8 weeks, splenic chimerisms were measured to assess the expansion of CFU-S. For a control, $CD34^+$ cells were directly transplanted without culturing on hPSCdBA layers (Figure 6A). As shown in Figure 6B, splenic chimerisms were significantly higher in hPSCdBA-cocultured $CD34^+$-transplanted mice than in mice with direct transplantation ($p = 0.041$; $n = 3$). Moreover, percentages of human CD33-positive myeloid cells were larger in cocultured $CD34^+$-transplanted mice (4.8 ± 0.13 versus 3.0 ± 0.19; $p = 0.00022$; $n = 3$, data not shown), while no significant changes in B lymphocyte percentages were observed (data not shown). These findings indicate that hPSCdBA serves as a stroma for MPCs, promoting their expansion/differentiation and homing to the spleen.

We also examined the expression of hematopoietic cytokines involved in the expansion and differentiation of committed HPCs. Various hematopoietin genes including thrombopoietin (*THPO*), *IL6*, *IL3*, colony-stimulating factor 3 (*CSF3*), colony-stimulating factor 2 (*CSF2*), and erythropoietin (*EPO*) were expressed in hESCdBA (Figure 6C, middle lanes) and hiPSCdWA (data not shown). On the other hand, hMSCdWAs expressed only *IL6* among these hemopoietins (Figure 6C, right lanes). Moreover, the expression levels of the hematopoietin genes in hESCdBA (Figure 6D) and hiPSCdBA (data not shown) were upregulated by isoproterenol treatments, further supporting the notion that hPSCdBA serves as stromal for committed HPCs.

To evaluate in vivo relevance, we examined whether isoproterenol treatment could enhance the recovery from antitumor agent-induced myelosuppression by enhancing the expansion/differentiation of MPCs. Mice were treated with 5-fluorouracile (5-FU), and bone marrow cells were collected and analyzed over time (Figure 6E). As reported by Hofer et al. (Hofer et al., 2007), 5-FU-treated mice were at the nadir at day 3, when a decline in total enucleated cell number (11.33 ± 1.74 versus 4.87 ± 0.96 [$\times 10^6$], $p = 0.0023$; $n = 3$) (Figure 6F) as well as a reduction in early myeloid cells (Figures S5A–S5C) were observed. Although total cell number (8.70 ± 0.40; $n = 3$) (Figure 6F) and the percentages of R1 fraction (Figures S5A and S5B) were eventually upregulated at day 7 as a sign of a recovery from myelosuppression, the mice still suffered from a shortage of mature myeloid cells (Figures S5A–S5C). By contrast, isoproterenol-treated mice showed higher enucleated cell number (10.93 ± 1.14, $p = 0.032$; $n = 3$) (Figure 6F) with significantly larger R2 fraction percentages (Figures S5A and S5B). Cytological studies confirmed all those findings (Figure S5C).

The existence of BA in BM has long been suggested despite the lack of direct evidence (reviewed in Motyl and Rosen, 2011). A relationship between osteoblast and BA was reported in mice (Calo et al., 2010). Moreover, murine BM fat reportedly expresses various BA-selective messages (Krings et al., 2012). To assess the possible existence of BA in human BM, expressions of BAT-specific markers, *UCP1* and *PRDM16*, were examined using commercially available human BM RNA samples. As shown in Figure 7A, expression of both genes was detected by RT-PCR, whereas they were undetectable in human BM-originated MSC-derived WA (hBM-MSCdWA). To further assess the existence of active BM-BAT in vivo, ^{18}F-FDG-PET/CT examinations were performed in healthy young volunteers (24.8 ± 5.8 of age; $n = 20$) with or without cold stimuli (Saito et al., 2009; Yoneshiro et al., 2011). We identified cold-stimulated ^{18}F-FDG uptake in vertebral BM (Figures 7B–7D), whose signal intensities showed an intimate correlation with those of BATs ($p < 0.001$), but not of those of brain, heart, spleen, or muscle (Figures S6A and S6B). The presence of vertebral BM was histologically examined using 3-week-old murine vertebral BM samples: we successfully detected the cells with BA morphologies (Figure 7E) that were positive for UCP1 protein expression (Figure 7F). Collectively, those findings strongly suggest the presence of functional BA in the BM of vertebrae.

DISCUSSION

We established a highly efficient method for the differentiation of hPSCs into functional BAs. This is the first success in generating functional classical BA pluripotent stem cells without exogenous gene transfer. By virtue of its technological merits, our method provides a valuable tool for BAT research. Functional

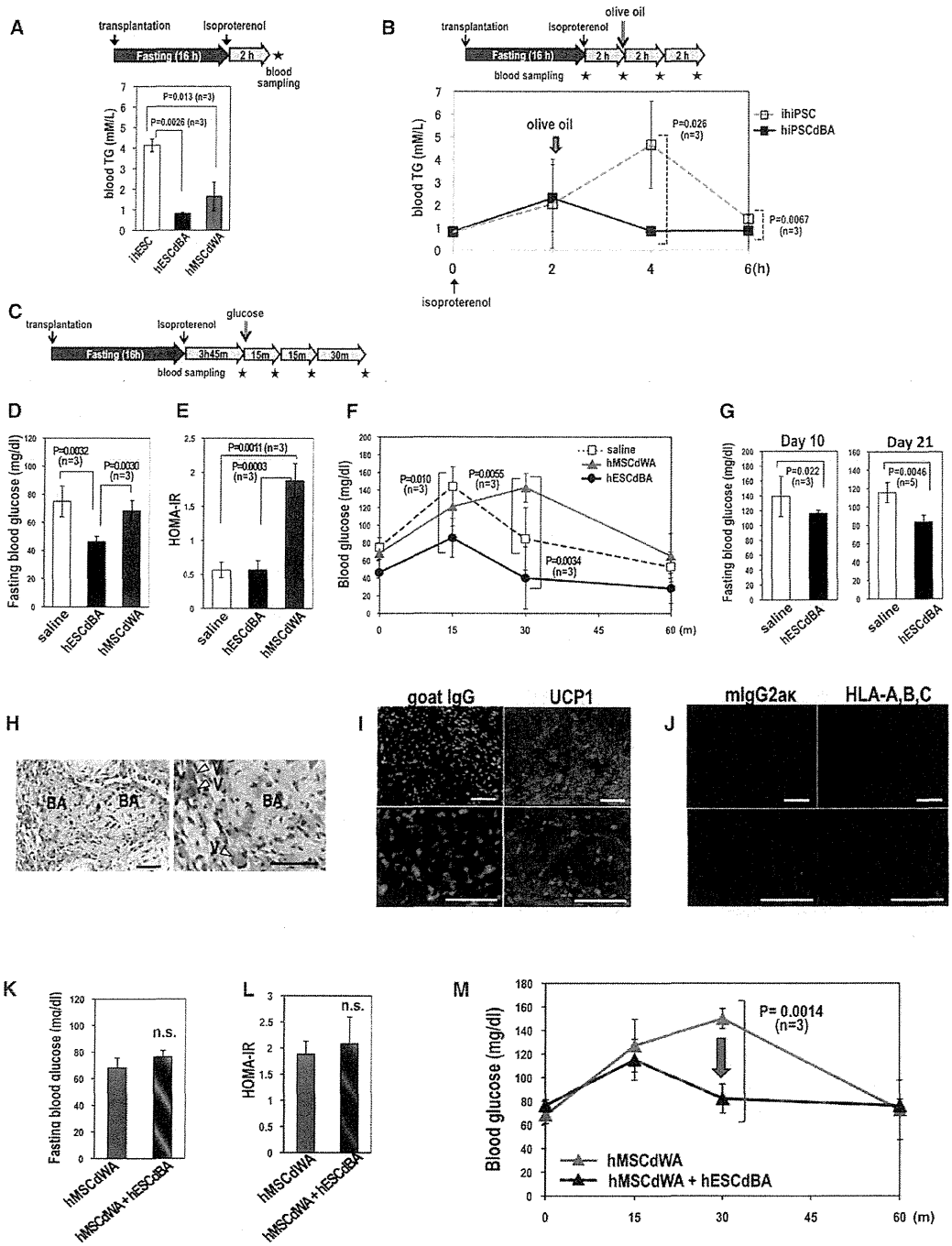

Figure 4. Metabolic Improvement by hPSC-Derived BA Transplantation

(A) Blood TG clearance tests. Immunocompetent ICR mice were transplanted with immature hESCs (ihESC) (n = 3 mice), hESCdBA (n = 3 mice), or hMSCdWA (n = 3 mice). After 16 hr starvation, isoproterenol was administrated and blood TG levels were measured.

(B) Oral fat tolerance tests. ICR mice were transplanted with immature hiPSC (ihiPSC) (n = 3 mice) or hiPSCdBA (n = 3 mice). Olive oil was orally loaded, and blood TG levels were measured over time after isoproterenol treatments.

(C–F) OGTT. ICR mice were injected with saline (n = 3 mice), hESCdBA (n = 3 mice), or hMSCdWA (n = 3 mice), and OGTT was performed (C). Fasting blood glucose levels (D), HOMA-IR (E), and blood glucose values after oral glucose loading (F) are shown.

(G–J) Immunocompromized NOG mice were injected with saline or transplanted with hESCdBA. At indicated time points, fasting blood glucose levels were measured. Three mice (day 10) or five mice (Day 21) were used for each condition (G). Histological studies were performed by HE staining (H) and

BA, which is responsible to a β3-adrenergic receptor agonist, has also been generated from human multipotent adipose-derived stem cells by chronic treatment with thiazolidinediones (Elabd et al., 2009). The merit of our system is that it does not require preparation of human specimen materials but utilizes hPSCs, which are capable of unlimited expansion in vitro.

One of the main findings of our research is that HC composed of KITLG, IL6, FLT3LG, and VEGF is essential for BA differentiation of hPSCs. Although BMP7 plays an important role in BA differentiation of hPSC (Figure S2) as reported in murine cases (Tseng et al., 2008), HC is indispensable for BA differentiation of hPSCs (Figure 1D). It is known that VEGF is synthesized in rodent BAT (Asano et al., 1997; Tonello et al., 1999), promoting the angiogenesis within BAT. Moreover, IL6 is reportedly secreted from cultured human BM adipocytes (Laharrague et al., 2000). Our findings imply that VEGF and IL6, together with KITLG and FLT3LG, work as fundamental autocrine or paracrine factors to promote BA differentiation.

Compatible to the finding by Sellayah et al. (Sellayah et al., 2011), the inhibitor analyses demonstrated the involvement of p38 MAPK signaling, but not of MEK signaling, in BA differentiation of hESC (Figures 5E–5G). However, distinct findings were obtained from the case of hiPSCs, in which MEK signaling played a role in BA differentiation (Figure 5E–5G). At this moment, the basis for the difference in the effects of identical inhibitors between hESCs and hiPSCs remains elusive. It may be related to the difference in the genetic background of pluripotent stem cell lines, reflecting the individual difference of the "donor" or the difference in the type of pluripotent stem cells or both. Further investigations are required to obtain the whole picture of the molecular basis for BA differentiation of hPSCs.

By providing high-purity human BA and WA materials, we demonstrated the differential effects on metabolic regulation between BA and WA: BA improves while WA deteriorates glucose metabolism. Because those effects were confirmed by a short-term assay without body weight changes and also because the effects of BA and WA on lipid metabolism were similar, the beneficial effect of BA on glucose metabolism is not a secondary consequence of general metabolic improvement. Conventional subcutaneous fat transplantation experiments were not able to distinguish the effect of BA from that of WA, because subcutaneous fat tissues contain both WA and BA. Thus, our system will provide a unique tool for the research of BA in regard to glucose metabolism.

Another surprising finding is the functional link between BA and hematopoiesis. We showed that hPSCdBAs serve as a stroma for MPCs. In contrast to the "niche" for HSCs, which is composed of immature osteoblasts and sinusoidal endothelial cells, the "stroma" for committed HPCs remains a mystery. The only report showing the characteristic of such stroma was a study by Dexter et al. (Dexter et al., 1977), in which BM fat cells with multilocular lipid droplets attached by mitochondria were identified as a stroma for CFU-S. Our results indicating that (1) hPSCdBAs express various hematopoietic cytokines in response to β-adrenergic receptor stimuli, (2) hPSCdBAs promote myelopoiesis of human cord blood $CD34^+$ cells, and (3) β-adrenergic receptor stimuli accelerate the recovery from 5-FU-mediated myelosuppression together show that BM-BAT serves as a stroma for MPCs. Among those, the third finding is particularly important because it illustrates a very feasible way to shorten the period of myelosuppression, the major side effect of intensive chemotherapy for progressive cancers.

The PET-CT results of young healthy volunteers, together with gene expression analyses of human BM specimen and histological examinations of murine vertebral BM samples, strongly suggest the existence of active BAT in vertebral BM in mammals. Because classical BAT is derived from *Myf5*-positive myoblastic cells (Seale et al., 2008) and because *Myf5*-positive cells emerge at the juxtaspinal, prospectively paravertebral, regions within somites (Cossu et al., 1996; Braun and Arnold, 1996), the existence of BA in vertebral BM seems reasonable. Because the major portions of vertebrae are composed of trabecular bones, which are the sites of active hematopoiesis, and the vertebral marrow is the last reserve site for hematopoietic activity in aged individuals (Tanaka and Inoue, 1976), the hematopoietic microenvironment of vertebral BM may bear a unique character. Further investigation will elucidate the whole picture of HPC regulation.

Our system, providing highly functional hiPSCdBA, may open a new avenue to the therapy for obesity. However, we have found that BA differentiation efficiencies substantially differ among hiPSC lines (data not shown), as reported in the case of pancreatic β cell differentiation of hESCs (Osafune et al., 2008). For clinical application, selection of appropriate lines of hiPSCs will be as important as sophisticating the whole differentiation process into good manufacturing practice levels.

EXPERIMENTAL PROCEDURES

Establishment of hiPSCs and Provision of hESCs

SeV-iPS cells were established from human neonatal fibroblast or human umbilical vein endothelial cells by introducing Yamanaka's four factors using CytoTune-iPS ver.1.0 (DNAVEC Corp) (Figure S7). Transgenes were eliminated by a 39þC heat treatment for 5 days. A hESC line (KhES-3) was generously provided by the Institute for Frontier Medical Science, Kyoto University (Suemori et al., 2006).

A Directed Differentiation of hESCs/hiPSCs into Functional BA

hESCs or hiPSCs were cultured in a 6 cm low-attachment culture dish using a serum-free differentiation medium composed of 1:1 ratio of IMDM (I3390, Sigma Chemical Co.) and Ham's F12 (087-08335, WAKO Pure Chemical Industries), 5 mg/ml bovine serum albumin (A802, Sigma Chemical Co.), 1:100 synthetic lipids (GIBCO #11905-031, Life Technologies, Inc.), 450 μM α- monothioglycerol (207-09232, WAKO Pure Chemical Industries), 1:100 insulin-transferrin-selenium (ITS-A, Life Technologies, Inc.), 2 mM Glutamax II (GIBCO #35050-061, Life Technologies, Inc.), 5% protein-free hybridoma mix (PFHMII, GIBCO #12040-077, Life Technologies, Inc.), 50 μg/ml ascorbic acid-2-phosphate (Sigma, A-8960), and the hematopoietic cytokine cocktail I (5 ng/ml IGF-II, 20 ng/ml BMP4, 5 ng/ml VEGFA, 20 ng/ml KITLG, 2.5 ng/ml FLT3LG, 2.5 ng/ml IL-6) for 8 days to form spheres. The

immunostaining using an anti-UCP1 antibody (I) and anti-human HLA-A,B,C antibody (J) at day 7. Arrowheads in (H) indicate microvasculatures. Scale bars, 50 μm.

(K–M) Mice were transplanted with hMSCdWAs alone or together with hESCdBA, and OGTT was performed. Fasting blood glucose levels (K), HOMA-IR (L), and blood glucose values after oral glucose loading (M) are shown. The error bars in (A), (B), (D)–(G), (K), (L), and (M) represent average ± SD.

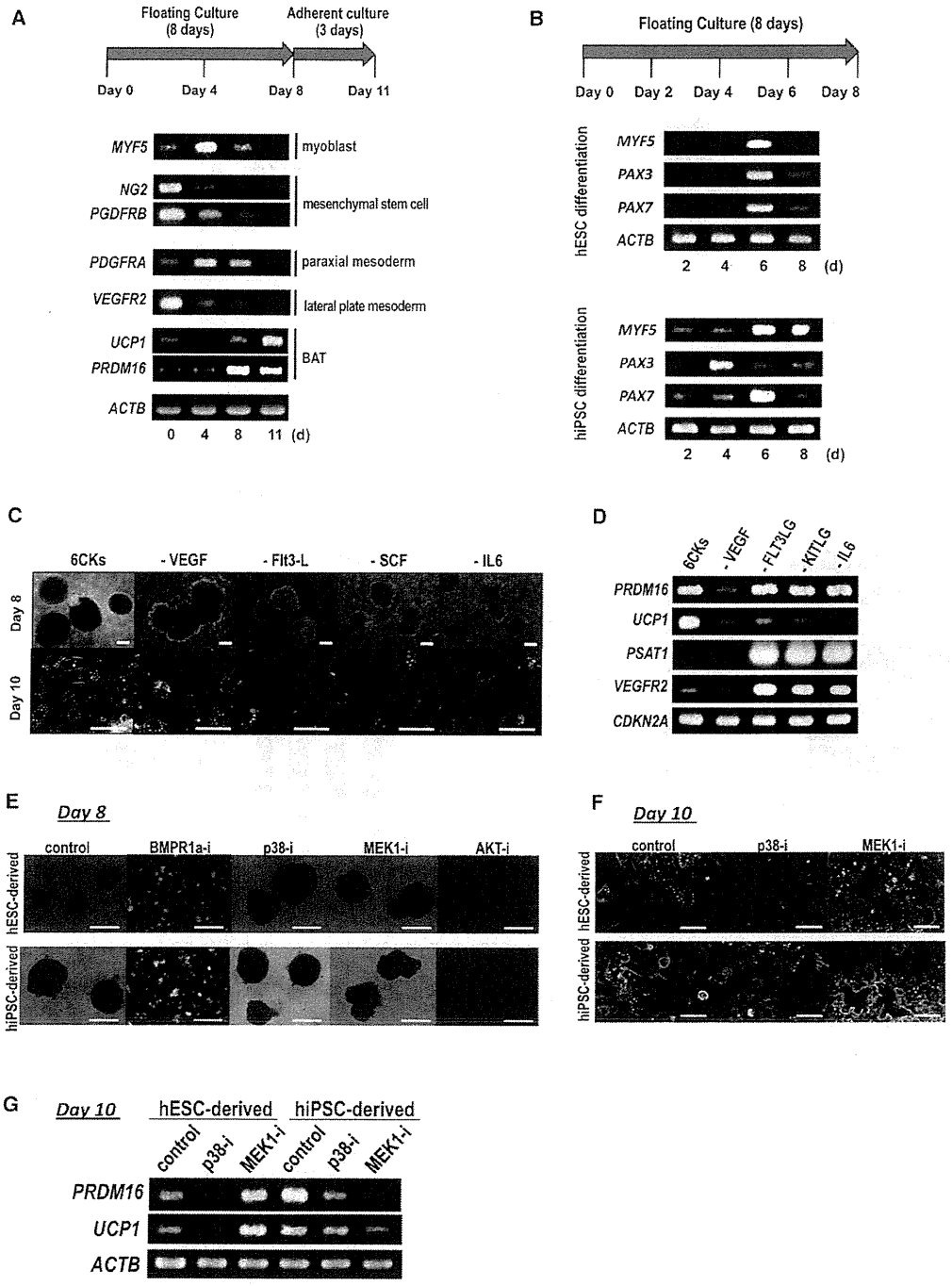

Figure 5. Signals Involved in BA Differentiation

(A) Developmental marker expression was examined by RT-PCR during BA differentiation of hESCs. Similar results were obtained regarding hiPSCs (data not shown).

(B) Myoblastic marker expressions were determined by RT-PCR during floating culture.

(C and D) The role of each cytokine was evaluated by morphological examinations (C) and RT-PCR (D). Scale bar, 100 μm (upper panels); and scale bar, 150 μm (lower panels).

(E–G) Inhibitor analyses. BA differentiation was performed in the presence of inhibitors of BMPR1a, p38 MAPK, MEK1, or AKT as indicated. Phase contrast micrographs of the spheres at day 8 (scale bar, 200 μm) (E) and those of BA at day 10 (scale bar, 50 μm) (F) were shown. Expressions of *UCP1* and *PRDM16* were determined at day 10 by RT-PCR (G).

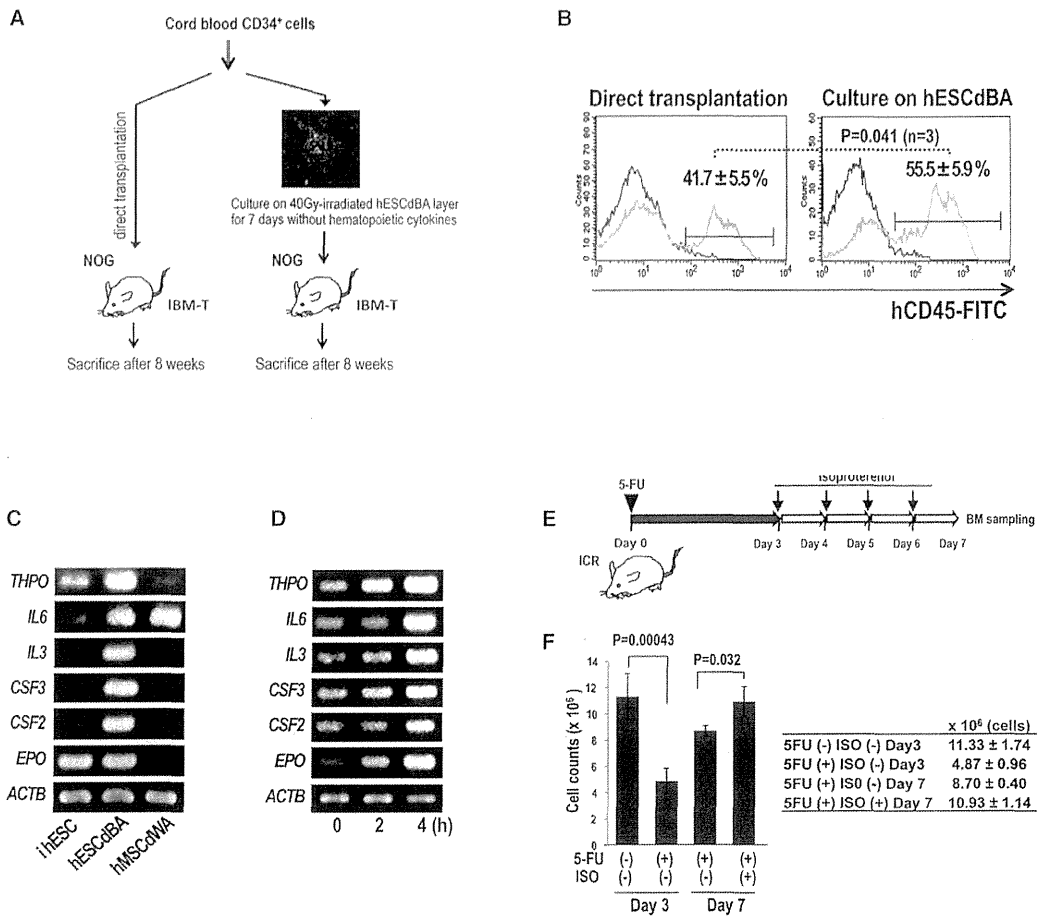

Figure 6. Hematopoietic Stromal Assays

(A) Schematic presentation of the assay.

(B) After 8 weeks from transplantation, cells were collected from the spleen and subjected to flow cytometry. hCD45-positive percentages were calculated. Similar results were obtained at 6 and 12 weeks after transplantation (data not shown). The error bars represent average ± SD (n = 3).

(C and D) Various hematopoietin expression was examined by RT-PCR in immature hESCs (ihESCs), hESCdBAs, and hMSCdWAs (C). Hematopoietin expression in hESCdBAs after isoproterenol treatments was examined over time by RT-PCR (D).

(E and F) 5-FU treatment assay. Experimental procedure (E) and the results of BM-enucleated cell counts (F) were shown. The error bars represent average ± SD (n = 3).

hESC/hiPSC-derived spheres were further cultured on gelatin-coated 6-well plates using the above-described serum-free medium supplemented with the hematopoietic cytokine cocktail II (5 ng/ml IGF-II, 10 ng/ml BMP7, 5 ng/ml VEGFA, 20 ng/ml KITLG, 2.5 ng/ml FLT3LG, 2.5 ng/ml IL-6) for several days.

Protein Expression Analyses

Immunostaining was performed using a goat polyclonal anti-human UCP1 antibody (sc-6528, Santa Cruz Biotechnology, Inc.) or a rabbit polyclonal anti-human SOD2 antibody LS-C39331, LifeSpan BioSciences Inc., Seattle, WA) as described previously (Nakahara et al., 2009). Western blotting was performed using a rabbit polyclonal UCP1 (Ab10983) (Abcam plc., Cambridge, UK) as described previously (Nakahara et al., 2009).

Gene Expression Analyses

RT-PCR was performed using primers described in Supplemental Information. Quantitative RT-PCR (qPCR) was performed by applying SYBR Green qPCR method using primers purchased from SuperArray (QIAGEN Science, Maryland, USA) as described in the Supplemental Experimental Procedures. The results were normalized by *GAPDH*.

Electron Microscopic Examinations

Cells were fixed by 2.5% glutaraldehyde. Postfixation by 2% osmium tetroxide, along with sample embedding into resin and slicing, was performed by Bio Medical Laboratories Co. Ltd. (Tokyo, Japan) (Saeki et al., 2000).

Inhibitor Analyses

BA differentiation was performed by adding the following inhibitors to the differentiation medium: 10 μM p38 MAP kinase inhibitor (Cat 506126) (Calbiochem Co., Darmstadt, Germany), 50 μM MEK1 inhibitor (PD 98059) (Calbiochem Co.), 10 μM BMPR1a inhibitor (Dorsomorphin Dihydrochloride, Cat 047-31801) (WAKO Pure Chemical Industries, Osaka, Japan), and 10 μM Akt inhibitor IV (Cat 124011) (Calbiochem Co.).

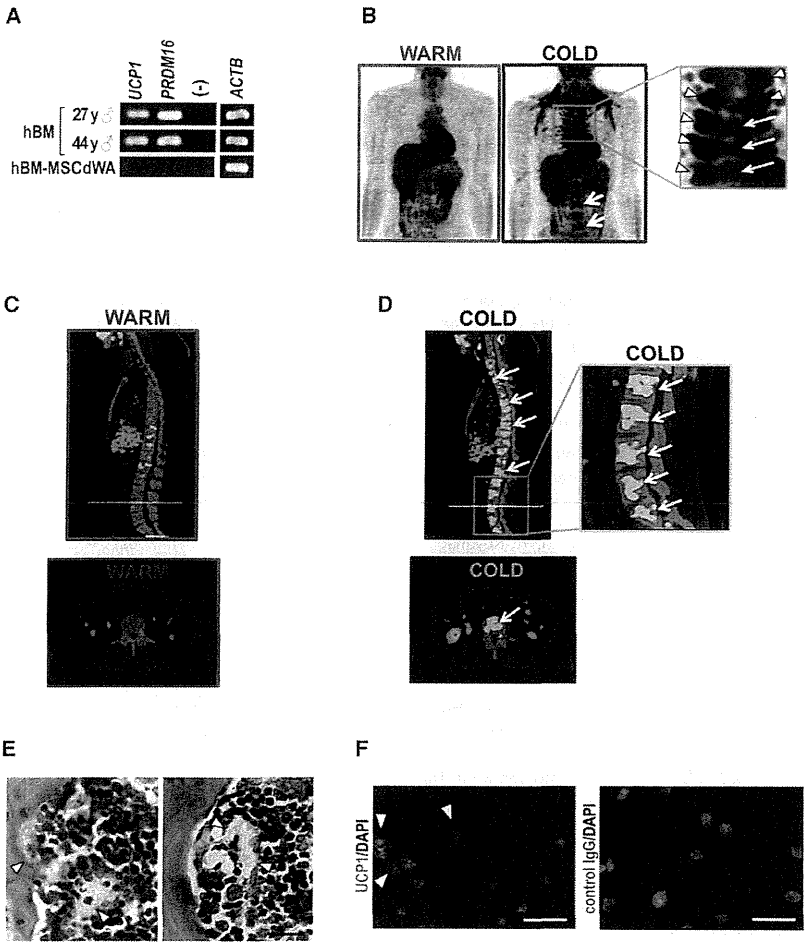

Figure 7. Examinations on BM-BAT

(A) Expression of *PRDM16* and *UCP1* in BM RNA samples of 27-year-old and 41-year-old males and human BM-derived hMSCdWA (hBM-MCdWA).

(B) ^{18}F-FDG-PET/CT. Typical results of the frontal images under warm and cold conditions were shown. Arrows indicate ^{18}F-FDG uptake into vertebrae per se, and arrowheads indicate ^{18}F-FDG uptake into classical paravertebral BA.

(C and D) Shown are sagittal and axial section images of ^{18}F-FDG-PET/CT under warm (C) and cold conditions (D). Arrows indicate the ^{18}F-FDG uptake into vertebral BM.

(E and F) Thoracic vertebra of 3-week-old ICR mice was subjected to HE staining (E) or UCP1 immunostaining (FF). Arrowheads indicate the existence of BA.

Oxygen Consumption Analyses

The adherent culture step of BA differentiation was performed on special 96-well plates (Seahorse Bioscience Inc., Billerica, MA) precoated by 0.1% gelatin by seeding 30 spheres per well. Oxygen consumption was analyzed by Extracellular Flux Analyzer XF96 (Seahorse Bioscience Inc.) according to the manufacturer's guidance.

Calorigenic Analyses

The 1 × 10^6 of hPSCdBA or immature hPSCs were suspended in 100 μl saline and subcutaneously transplanted into 5-week-old male ICR mice After 24 hr, 30 μmol/kg of isoproterenol (12760, Sigma Chemical Co.) was administrated from the tail vein. After another 4 hr, mice were anesthetized, and dermal temperature was measured by Thermo GEAR G120/G100 (NEC Avio Infrared Technologies Co., Ltd, Tokyo, Japan). All animal care procedures involved in calorigenic analyses, assessment of lipid and metabolism, and hematopoietic stromal assays were approved by the Animal Care and Use Committee of the Research Institute, National Center for Global Health and Medicine (NCGM), and complied with the procedures of the Guide for the Care and Use of Laboratory Animals of NCGM.

Assessment of Lipid Metabolism

Six-week-old male CR mice were subcutaneously transplanted with 1 × 10^6 of immature hESC, hESCdBA, or hMC-derived WA suspended in 100 μl saline and kept abstained from feed. After 16 hr, isoproterenol (30 μmol/kg) was administrated. After another 2 hr, blood samples were taken, and TG concentrations were measured by Accutrend Plus (F. Hoffmann-La Roche, Ltd., Basel, Switzerland). For oral fat tolerance tests, ICR mice were subcutaneously transplanted with immature hPSC or hPSCdBA and kept abstained from feed. After 16 hr, isoproterenol (15 μmol/kg) was administrated. After another 2 hr, 200 μl of olive oil was orally administrated, and blood TG levels were measured every 2 hr.

Assessment of Glucose Metabolism

The 1 × 10^6 of hESCdBA or hMSCdWA was transplanted to 6- or 10-week-old male ICR mice, which were kept abstained from feed. After 16 hr, isoproterenol (30 μmol/kg) was administrated. After another 4 hr, 2 g/kg of glucose (041-00595, Wako Pure Chemical Industries, Ltd., Osaka, Japan) was orally administrated. Blood sample were taken after 0, 15, 30, and 60 min. Blood glucose concentrations were measured by Accutrend Plus, and plasma insulin concentrations were measured by mouse insulin ELISA kit (Morinaga Institute of Biological Science, Inc., Yokohama, Japan).

Hematopoietic Stromal Assays

The human cord blood CD34$^+$ cells were cultured on hPSCdBA layers without recombinant cytokines in RPMI1640 medium supplemented with 10% fetal calf serum. Floating cells were collected after 7 days, and 2 × 10^5 cells were transplanted into tibial bone marrow of NOG mice. After 6, 8, and 12 weeks, cells were collected from contralateral femoral bone marrow and spleen and subjected to cytometry using an anti-human CD45-FITC (clone J33) (Beckman Coulter Inc.) and anti-human CD33-PE antibody (clone WM53) (BD Biosciences, San Jose, CA). For control, cord blood CD34$^+$ cells were directly transplanted without coculture. For myelosuppression recovery assays, 100 mg/kg of 5-FU was intraperitoneally administrated. From day 3 to day 6, 30 μmol/kg of isoproterenol was administrated from tail vein. At day 7, bone marrow cells were collected from femoral bones and analyzed.

^{18}F-FDG-PET/CT Examinations

After careful instruction regarding the study and informed consent to participants, PET/CT examinations of healthy young volunteers (24.8 ± 5.8 years of age, n = 20) were performed. The protocol was approved by the institutional review boards of Tenshi College. Standardized uptake value (SUV) was measured by an expert as described in the Supplemental Experimental Procedures. Data are reported as means ± SEM. Statistics analyses were performed using SPSS software, version 18 (International Business Machines

Corp, New York), as described in the Supplemental Experimental Procedures. P values are considered to be statistically significant if <0.05.

SUPPLEMENTAL INFORMATION

Supplemental Information includes seven figures, Supplemental Experimental Procedures, and Supplemental References and can be found with this article online at http://dx.doi.org/10.1016/j.cmet.2012.08.001.

ACKNOWLEDGMENTS

This work was supported by Grant-in-Aid from Ministry of Health, Labour and Welfare of Japan (KHD1017) and by Japan Science and Technology Agency (AS 2321379G). We thank Mr. Kameya at LSI Sapporo Clinic for technical assistance for PET-CT examinations and Mr. Obara at LSI Sapporo Clinic for general assistance.

Received: March 17, 2012
Revised: June 30, 2012
Accepted: August 1, 2012
Published online: September 4, 2012

REFERENCES

Ahfeldt, T., Schinzel, R.T., Lee, Y.K., Hendrickson, D., Kaplan, A., Lum, D.H., Camahort, R., Xia, F., Shay, J., Rhee, E.P., et al. (2012). Programming human pluripotent stem cells into white and brown adipocytes. Nat. Cell Biol. *14*, 209–219.

Arai, F., and Suda, T. (2007). Maintenance of quiescent hematopoietic stem cells in the osteoblastic niche. Ann. N Y Acad. Sci. *1106*, 41–53.

Asano, A., Morimatsu, M., Nikami, H., Yoshida, T., and Saito, M. (1997). Adrenergic activation of vascular endothelial growth factor mRNA expression in rat brown adipose tissue: implication in cold-induced angiogenesis. Biochem. J. *328*, 179–183.

Bartelt, A., Bruns, O.T., Reimer, R., Hohenberg, H., Ittrich, H., Peldschus, K., Kaul, M.G., Tromsdorf, U.I., Weller, H., Waurisch, C., et al. (2011). Brown adipose tissue activity controls triglyceride clearance. Nat. Med. *17*, 200–205.

Braun, T., and Arnold, H.H. (1996). Myf-5 and myoD genes are activated in distinct mesenchymal stem cells and determine different skeletal muscle cell lineages. EMBO J. *15*, 310–318.

Calo, E., Quintero-Estades, J.A., Danielian, P.S., Nedelcu, S., Berman, S.D., and Lees, J.A. (2010). Rb regulates fate choice and lineage commitment in vivo. Nature *466*, 1110–1114.

Cossu, G., Kelly, R., Tajbakhsh, S., Di Donna, S., Vivarelli, E., and Buckingham, M. (1996). Activation of different myogenic pathways: myf-5 is induced by the neural tube and MyoD by the dorsal ectoderm in mouse paraxial mesoderm. Development *122*, 429–437.

Crisan, M., Yap, S., Casteilla, L., Chen, C.W., Corselli, M., Park, T.S., Andriolo, G., Sun, B., Zheng, B., Zhang, L., et al. (2008). A perivascular origin for mesenchymal stem cells in multiple human organs. Cell Stem Cell *3*, 301–313.

Cypess, A.M., Lehman, S., Williams, G., Tal, I., Rodman, D., Goldfine, A.B., Kuo, F.C., Palmer, E.L., Tseng, Y.H., Doria, A., et al. (2009). Identification and importance of brown adipose tissue in adult humans. N. Engl. J. Med. *360*, 1509–1517.

Dexter, T.M., Allen, T.D., and Lajtha, L.G. (1977). Conditions controlling the proliferation of haemopoietic stem cells in vitro. J. Cell. Physiol. *91*, 335–344.

Elabd, C., Chiellini, C., Carmona, M., Galitzky, J., Cochet, O., Petersen, R., Pénicaud, L., Kristiansen, K., Bouloumié, A., Casteilla, L., et al. (2009). Human multipotent adipose-derived stem cells differentiate into functional brown adipocytes. Stem Cells *27*, 2753–2760.

Enerbäck, S., Jacobsson, A., Simpson, E.M., Guerra, C., Yamashita, H., Harper, M.E., and Kozak, L.P. (1997). Mice lacking mitochondrial uncoupling protein are cold-sensitive but not obese. Nature *387*, 90–94.

Feldmann, H.M., Golozoubova, V., Cannon, B., and Nedergaard, J. (2009). UCP1 ablation induces obesity and abolishes diet-induced thermogenesis in mice exempt from thermal stress by living at thermoneutrality. Cell Metab. *9*, 203–209.

Gimble, J.M., Dorheim, M.A., Cheng, Q., Medina, K., Wang, C.S., Jones, R., Koren, E., Pietrangeli, C., and Kincade, P.W. (1990). Adipogenesis in a murine bone marrow stromal cell line capable of supporting B lineage lymphocyte growth and proliferation: biochemical and molecular characterization. Eur. J. Immunol. *20*, 379–387.

Gimble, J.M., Youkhana, K., Hua, X., Bass, H., Medina, K., Sullivan, M., Greenberger, J., and Wang, C.S. (1992). Adipogenesis in a myeloid supporting bone marrow stromal cell line. J. Cell. Biochem. *50*, 73–82.

Gupta, R.K., Mepani, R.J., Kleiner, S., Lo, J.C., Khandekar, M.J., Cohen, P., Frontini, A., Bhowmick, D.C., Ye, L., Cinti, S., et al. (2012). Zfp423 expression identifies committed preadipocytes and localizes to adipose endothelial and perivascular cells. Cell Metab. *15*, 230–239.

Hiroyama, T., Miharada, K., Aoki, N., Fujioka, T., Sudo, K., Danjo, I., Nagasawa, T., and Nakamura, Y. (2006). Long-lasting in vitro hematopoiesis derived from primate embryonic stem cells. Exp. Hematol. *34*, 760–769.

Hofer, M., Pospísil, M., Znojil, V., Holá, J., Vacek, A., and Streitová, D. (2007). Adenosine A(3) receptor agonist acts as a homeostatic regulator of bone marrow hematopoiesis. Biomed. Pharmacother. *61*, 356–359.

Ito, M., Hiramatsu, H., Kobayashi, K., Suzue, K., Kawahata, M., Hioki, K., Ueyama, Y., Koyanagi, Y., Sugamura, K., Tsuji, K., et al. (2002). NOD/SCID/gamma(c)(null) mouse: an excellent recipient mouse model for engraftment of human cells. Blood *100*, 3175–3182.

Jacene, H.A., Cohade, C.C., Zhang, Z., and Wahl, R.L. (2011). The relationship between patients' serum glucose levels and metabolically active brown adipose tissue detected by PET/CT. Mol. Imaging Biol. *13*, 1278–1283.

Jackson, D.M., Hambly, C., Trayhurn, P., and Speakman, J.R. (2001). Can non-shivering thermogenesis in brown adipose tissue following NA injection be quantified by changes in overlying surface temperatures using infrared thermography? J. Therm. Biol. *26*, 85–93.

Kiel, M.J., and Morrison, S.J. (2006). Maintaining hematopoietic stem cells in the vascular niche. Immunity *25*, 862–864.

Kontani, Y., Wang, Y., Kimura, K., Inokuma, K.I., Saito, M., Suzuki-Miura, T., Wang, Z., Sato, Y., Mori, N., and Yamashita, H. (2005). UCP1 deficiency increases susceptibility to diet-induced obesity with age. Aging Cell *4*, 147–155.

Krings, A., Rahman, S., Huang, S., Lu, Y., Czernik, P.J., and Lecka-Czernik, B. (2012). Bone marrow fat has brown adipose tissue characteristics, which are attenuated with aging and diabetes. Bone *50*, 546–552.

Laharrague, P., Fontanilles, A.M., Tkaczuk, J., Corberand, J.X., Pénicaud, L., and Casteilla, L. (2000). Inflammatory/haematopoietic cytokine production by human bone marrow adipocytes. Eur. Cytokine Netw. *11*, 634–639.

Motyl, K.J., and Rosen, C.J. (2011). Temperatures rising: brown fat and bone. Discov. Med. *11*, 179–185.

Nagasawa, T. (2007). The chemokine CXCL12 and regulation of HSC and B lymphocyte development in the bone marrow niche. Adv. Exp. Med. Biol. *602*, 69–75.

Nakahara, M., Nakamura, N., Matsuyama, S., Yogiashi, Y., Yasuda, K., Kondo, Y., Yuo, A., and Saeki, K. (2009). High-efficiency production of subculturable vascular endothelial cells from feeder-free human embryonic stem cells without cell-sorting technique. Cloning Stem Cells *11*, 509–522.

Naveiras, O., Nardi, V., Wenzel, P.L., Hauschka, P.V., Fahey, F., and Daley, G.Q. (2009). Bone-marrow adipocytes as negative regulators of the haematopoietic microenvironment. Nature *460*, 259–263.

Ookura, N., Fujimori, Y., Nishioka, K., Kai, S., Hara, H., and Ogawa, H. (2007). Adipocyte differentiation of human marrow mesenchymal stem cells reduces the supporting capacity for hematopoietic progenitors but not for severe combined immunodeficiency repopulating cells. Int. J. Mol. Med. *19*, 387–392.

Osafune, K., Caron, L., Borowiak, M., Martinez, R.J., Fitz-Gerald, C.S., Sato, Y., Cowan, C.A., Chien, K.R., and Melton, D.A. (2008). Marked differences in differentiation propensity among human embryonic stem cell lines. Nat. Biotechnol. *26*, 313–315.

Ouellet, V., Routhier-Labadie, A., Bellemare, W., Lakhal-Chaieb, L., Turcotte, E., Carpentier, A.C., and Richard, D. (2011). Outdoor temperature, age, sex, body mass index, and diabetic status determine the prevalence, mass, and glucose-uptake activity of 18F-FDG-detected BAT in humans. J. Clin. Endocrinol. Metab. *96*, 192–199.

Petrovic, N., Walden, T.B., Shabalina, I.G., Timmons, J.A., Cannon, B., and Nedergaard, J. (2010). Chronic peroxisome proliferator-activated receptor gamma (PPARgamma) activation of epididymally derived white adipocyte cultures reveals a population of thermogenically competent, UCP1-containing adipocytes molecularly distinct from classic brown adipocytes. J. Biol. Chem. *285*, 7153–7164.

Reznikoff, C.A., Brankow, D.W., and Heidelberger, C. (1973). Establishment and characterization of a cloned line of C3H mouse embryo cells sensitive to postconfluence inhibition of division. Cancer Res. *33*, 3231–3238.

Saeki, K., Yuo, A., Okuma, E., Yazaki, Y., Susin, S.A., Kroemer, G., and Takaku, F. (2000). Bcl-2 down-regulation causes autophagy in a caspase-independent manner in human leukemic HL60 cells. Cell Death Differ. *7*, 1263–1269.

Saito, M., Okamatsu-Ogura, Y., Matsushita, M., Watanabe, K., Yoneshiro, T., Nio-Kobayashi, J., Iwanaga, T., Miyagawa, M., Kameya, T., Nakada, K., et al. (2009). High incidence of metabolically active brown adipose tissue in healthy adult humans: effects of cold exposure and adiposity. Diabetes *58*, 1526–1531.

Sakurai, H., Era, T., Jakt, L.M., Okada, M., Nakai, S., Nishikawa, S., and Nishikawa, S. (2006). In vitro modeling of paraxial and lateral mesoderm differentiation reveals early reversibility. Stem Cells *24*, 575–586.

Seale, P., Kajimura, S., Yang, W., Chin, S., Rohas, L.M., Uldry, M., Tavernier, G., Langin, D., and Spiegelman, B.M. (2007). Transcriptional control of brown fat determination by PRDM16. Cell Metab. *6*, 38–54.

Seale, P., Bjork, B., Yang, W., Kajimura, S., Chin, S., Kuang, S., Scimè, A., Devarakonda, S., Conroe, H.M., Erdjument-Bromage, H., et al. (2008). PRDM16 controls a brown fat/skeletal muscle switch. Nature *454*, 961–967.

Sellayah, D., Bharaj, P., and Sikder, D. (2011). Orexin is required for brown adipose tissue development, differentiation, and function. Cell Metab. *14*, 478–490.

Suemori, H., Yasuchika, K., Hasegawa, K., Fujioka, T., Tsuneyoshi, N., and Nakatsuji, N. (2006). Efficient establishment of human embryonic stem cell lines and long-term maintenance with stable karyotype by enzymatic bulk passage. Biochem. Biophys. Res. Commun. *345*, 926–932.

Sun, L., Xie, H., Mori, M.A., Alexander, R., Yuan, B., Hattangadi, S.M., Liu, Q., Kahn, C.R., and Lodish, H.F. (2011). Mir193b-365 is essential for brown fat differentiation. Nat. Cell Biol. *13*, 958–965.

Takayama, N., Nishikii, H., Usui, J., Tsukui, H., Sawaguchi, A., Hiroyama, T., Eto, K., and Nakauchi, H. (2008). Generation of functional platelets from human embryonic stem cells in vitro via ES-sacs, VEGF-promoted structures that concentrate hematopoietic progenitors. Blood *111*, 5298–5306.

Tanaka, Y., and Inoue, T. (1976). Fatty marrow in the vertebrae. A parameter for hematopoietic activity in the aged. J. Gerontol. *31*, 527–532.

Thorns, C., Schardt, C., Katenkamp, D., Kähler, C., Merz, H., and Feller, A.C. (2008). Hibernoma-like brown fat in the bone marrow: report of a unique case. Virchows Arch. *452*, 343–345.

Timmons, J.A., Wennmalm, K., Larsson, O., Walden, T.B., Lassmann, T., Petrovic, N., Hamilton, D.L., Gimeno, R.E., Wahlestedt, C., Baar, K., et al. (2007). Myogenic gene expression signature establishes that brown and white adipocytes originate from distinct cell lineages. Proc. Natl. Acad. Sci. USA *104*, 4401–4406.

Tonello, C., Giordano, A., Cozzi, V., Cinti, S., Stock, M.J., Carruba, M.O., and Nisoli, E. (1999). Role of sympathetic activity in controlling the expression of vascular endothelial growth factor in brown fat cells of lean and genetically obese rats. FEBS Lett. *442*, 167–172.

Tran, K.V., Gealekman, O., Frontini, A., Zingaretti, M.C., Morroni, M., Giordano, A., Smorlesi, A., Perugini, J., De Matteis, R., Sbarbati, A., et al. (2012). The vascular endothelium of the adipose tissue gives rise to both white and brown fat cells. Cell Metab. *15*, 222–229.

Tseng, Y.H., Kokkotou, E., Schulz, T.J., Huang, T.L., Winnay, J.N., Taniguchi, C.M., Tran, T.T., Suzuki, R., Espinoza, D.O., Yamamoto, Y., et al. (2008). New role of bone morphogenetic protein 7 in brown adipogenesis and energy expenditure. Nature *454*, 1000–1004.

van Marken Lichtenbelt, W.D., Vanhommerig, J.W., Smulders, N.M., Drossaerts, J.M., Kemerink, G.J., Bouvy, N.D., Schrauwen, P., and Teule, G.J. (2009). Cold-activated brown adipose tissue in healthy men. N. Engl. J. Med. *360*, 1500–1508.

Virtanen, K.A., Lidell, M.E., Orava, J., Heglind, M., Westergren, R., Niemi, T., Taittonen, M., Laine, J., Savisto, N.J., Enerbäck, S., and Nuutila, P. (2009). Functional brown adipose tissue in healthy adults. N. Engl. J. Med. *360*, 1518–1525.

Yoneshiro, T., Aita, S., Matsushita, M., Okamatsu-Ogura, Y., Kameya, T., Kawai, Y., Miyagawa, M., Tsujisaki, M., and Saito, M. (2011). Age-related decrease in cold-activated brown adipose tissue and accumulation of body fat in healthy humans. Obesity (Silver Spring) *19*, 1755–1760.

Original Article

DOI: 10.5582/bst.2012.v6.2.70

Analysis of cytotoxicity induced by proinflammatory cytokines in the human alveolar epithelial cell line A549

Mitsuaki Muroya, Kyungho Chang*, Kanji Uchida, Masahiko Bougaki, Yoshitsugu Yamada

Department of Anesthesiology, Faculty of Medicine, The University of Tokyo, Tokyo, Japan.

Summary **Epithelial cell injury under hyperinflammatory conditions is critical in the development of septic acute lung injury (ALI). The aim of the present study is to analyze the cytotoxic effects of a mixture of proinflammatory cytokines in the human alveolar epithelial cell line A549. The cytotoxicity of proinflammatory cytokines were assessed in A549 cells by measuring lactate dehydrogenase released into the culture medium and by crystal violet staining of surviving cells. Activation of the caspase-dependent apoptotic pathway was evaluated by monitoring cleavage of cytokeratin 18 by caspases using enzyme-liked immunosorbent assay (ELISA). To estimate the cytotoxic signaling pathways responsible for epithelial injury, agents with antiinflammatory or antioxidative properties were extensively screened for cytoprotective effects in the inflammation-associated epithelial injury model. The present study revealed that inflammatory cytokines exerted cytotoxicity in A549 cells. A mixture of interleukin-1beta (IL-1β), tumor necrosis factor-alpha (TNF-α) and interferon-gamma (IFN-γ), designated as cytomix, augmented cytotoxicity compared with each individual cytokine. Treatment with glucocorticoid (dexamethasone), tetracycline-derived antiinflammatory antibiotics (minocycline or doxycycline), angiotensin II receptor blockers (losartan or telmisartan), or antioxidants (dimethyl sulfoxide, catalase) attenuated cytomix-induced cytotoxicity, including caspase activation. These results implied that inflammatory cytokines alone could cause alveolar epithelial injury in the pathophysiology of septic ALI. Caspase-dependent apoptosis was speculated to be one mechanism responsible for the cytokine-induced cytotoxicity. Agents with antiinflammatory or antioxidative properties such as glucocorticoid, tetracycline-derived antibiotics, angiotensin II receptor blockers, or direct antioxidants showed substantial effect in attenuating cytokine-induced cytotoxicity and may be candidates for treatment options.**

Keywords: Acute lung injury, sepsis, proinflammatory cytokine, epithelial cell injury, apoptosis

1. Introduction

Despite the broad repertoire of potent antibiotics and progress in intensive patient care, sepsis remains a life-threatening condition (*1*). Multiple organ dysfunctions are responsible for the high mortality rate of septic patients. Pulmonary, renal, cardiovascular and coagulation systems are susceptible to acute injury during septic sequelae and therefore resolution of vital organ dysfunctions is pivotal in management of patients with sepsis (*2*). Acute lung injury (ALI) and its more severe form, acute respiratory distress syndrome (ARDS), are characterized by hypoxemia and diffuse bilateral infiltrates in the lung (*3*). Although protective ventilatory strategies have been reported to improve patient survival (*4*), core information leading to decisive therapeutic intervention is still lacking. The pathophysiological basis of ALI consists of excessive and protracted alveolar inflammation accompanied by alveolar epithelial injury, including epithelial cell death (*5-7*). Thus, it is critical to clarify

*Address correspondence to:
Dr. Kyungho Chang, Department of Anesthesiology, Faculty of medicine, The University of Tokyo, Hongo 7-3-1, Bunkyo-ku, Tokyo 113-8655, Japan.
E-mail: kchang-tky@umin.ac.jp

how the hyperinflammatory condition damages alveolar epithelial cells and to explore what pharmacological agents have potential to protect lung tissue.

In this study, we evaluated the cytotoxicity induced by a mixture of proinflammatory cytokines (IL-1β/TNF-α/IFN-γ), which have been suggested to play major roles in sepsis or ALI (*5,8-13*), in the human alveolar epithelial cell line A549. Then, to clarify the cytotoxic signaling pathways responsible for alveolar epithelial cell injury, various agents with antiinflammatory or antioxidative properties were screened for cytoprotective effects in an *in vitro* acute lung injury model (*9,14-17*).

2. Materials and Methods

2.1. *Cell culture and reagents*

Human lung carcinoma type II epithelium-like A549 cells, purchased from Riken BioResource Center Cell Bank (Tsukuba, Ibaraki, Japan), were grown in Dulbecco's Modified Eagle's Medium (DMEM; Sigma, St. Louis, MO, USA) with 10% heat-inactivated fetal bovine serum (FBS), 100 U/mL penicillin, 100 mg/mL streptomycin in 10 cm dishes at 37°C in a humidified atmosphere of 5% CO_2.

Reagents were purchased commercially as follows; human IL-1β, human high-mobility group box 1 (Humanzyme, Chicago, IL, USA); human TNF-α, human interleukin-6 (IL-6) (Prospec, Rehovot, Israel), human IFN-γ (Peprotech, Rocky Hill, NJ, USA); dexamethasone, minocycline, doxycycline, human Fas ligand (Enzo, Plymouth Meeting, PA, USA); losartan, telmisartan (LKT Laboratories, St. Paul, MN, USA); dimethyl sulfoxide (DMSO), catalase-polyethylene glycol (PEG), crystal violet (Sigma, St. Louis, MO, USA).

2.2. *Drug treatment*

A549 cells were seeded in 24-well tissue culture plates at 5×10^4 cells/well overnight. After cell attachment, the content of FBS in medium was decreased to 2% by medium change. Cells were pretreated for 1 h with agents which were expected to confer cytoprotection and then stimulated with proinflammatory cytokines. To recapitulate the severe inflammatory condition *in vitro* experiments, stimulation of cultured cells by combination of proinflammatory cytokines, such as IL-1β/TNF-α/IFN-γ (designated as cytomix for convenience) was employed (*15-17*). The concentration of these cytokines was mainly 10 ng/mL in the present study. This value was adopted with reference to other reports (*15-17*) and to our preliminary experiments. In fact, at this concentration, either IL-1β or TNF-α exerted substantial cytotoxicity in A549 cells. Control (ctrl) cells were treated with the corresponding vehicle alone. The concentration of vehicle DMSO or ethanol in the medium was kept ≤ 0.2% to minimize the effect of solvents.

2.3. *Cytotoxicity of cytokines against A549 cells*

The cytotoxicity of cytokines against A549 cells was evaluated after 24 h-60 h of cytokine stimulation depending on the purpose of the experiments. Cell morphologies were observed and photographed under a light microscope. Cytotoxicity was evaluated quantitatively by monitoring lactate dehydrogenase (LDH) concentration in culture medium and by crystal violet staining (*18,19*). LDH is abundant in the cytoplasm and is released into the culture medium accompanying damage of the cell membrane. Crystal violet solution can promptly fix and stain living cells on culture plates. Thus, LDH concentration reflects the total amount of damaged cells, while crystal violet staining reflects the total amount of surviving cells.

2.3.1. *LDH determination*

LDH concentration in culture medium was determined using a Cytotoxicity Detection Kit Plus (Roche Applied Science, Mannheim, Germany) according to the manufacturer's instructions. The samples were measured spectrophotometrically at a wavelength of 490 nm (with a reference wavelength of 620 nm). After subtracting the background control value (medium only), each sample value was represented in relation to the untreated control value.

2.3.2. *Crystal violet staining*

After aspiration of culture medium, surviving cells were fixed and stained with 0.5% crystal violet in 95% ethanol for 5 min and then washed with tap water several times. After photographs were taken, 1% sodium dodecylsulfate (SDS) solution was added to each well to elute the blue dye and the absorbance at 595 nm of the eluted samples was measured spectrophotometrically for quantitative evaluation. The values of samples stimulated with cytomix in the presence of pretreatment drugs were calibrated relative to that of the corresponding control with pretreatment drug only.

2.3.3. *Evaluation of caspase activity*

To explore the contribution of apoptosis to the cytokine-induced cytotoxicity of A549 cells, caspase activity was investigated. To this purpose, the levels of soluble caspase-cleaved cytokeratin 18 fragments were measured by M30 cytodeath ELISA (Peviva, Bromma, Sweden) according to the manufacturer's instructions. The M30 antibody recognizes a neo-epitope (Asp396) exposed after cleavage of cytokeratin 18 by effector caspase (caspase 3, 6, and 7) in human, monkey, and

bovine epithelial cells (*20,21*). After subtracting the background control value (empty blank), each sample value was represented in relation to the untreated control value.

2.4. *Statistical analysis*

Experiments were carried out in triplicate and repeated at least three times. Data are expressed as means ± standard error of mean (S.E.M.). Statistical significance of differences between means was determined with either by Student's *t* test or by analysis of variance followed by post hoc Tukey test for multiple comparisons. All statistical procedures were performed using Excel 2004 (Microsoft, USA) with the add-in software Statmate™ 2008 (ATMS, Japan). In all analyses, $p < 0.05$ was taken to indicate statistical significance.

3. Results

3.1. *Mixture of proinflammatory cytokines exerted cytotoxicity synergistically in A549 cells*

The cytotoxic effects of proinflammatory cytokines were investigated in A549 cells. Cytomix (a mixture of IL-1β/TNF-α/IFN-γ) induced cell death, a decrease in cell number, and morphological changes in A549 cells in a dose dependent manner (Figures 1A and 1B). The cytotoxicity became prominent 48 hours after cytomix challenge (Figure 1C). IL-1β decreased cell survival (Figures 2A and 2B) and significantly induced cell damage (Figure 2C). TNF-α showed similar cytotoxicity, although to a lesser extent than IL-1β at the same concentration. IFN-γ alone failed to show cytotoxicity at this concentration. However, adding IFN-γ to IL-1β/TNF-α significantly augmented the cytotoxicity compared to IL-1β/TNF-α alone. This cytotoxic synergism was thought to reflect the clinical observations in sepsis where multiple cytokines are responsible for biological toxic effects in cooperation (*22*).

To estimate the role of apoptosis in cytokine-induced cytotoxicity, the activity of caspases was evaluated by measurement of cleaved cytokeratin 18 released into the culture medium. Cytokeratin 18 is a cytoskeleton protein distributed in the cytoplasm of human epithelial cells. It is a substrate of activated effector caspases (caspase 3, 6, 7), and the amount of cleaved form in culture medium

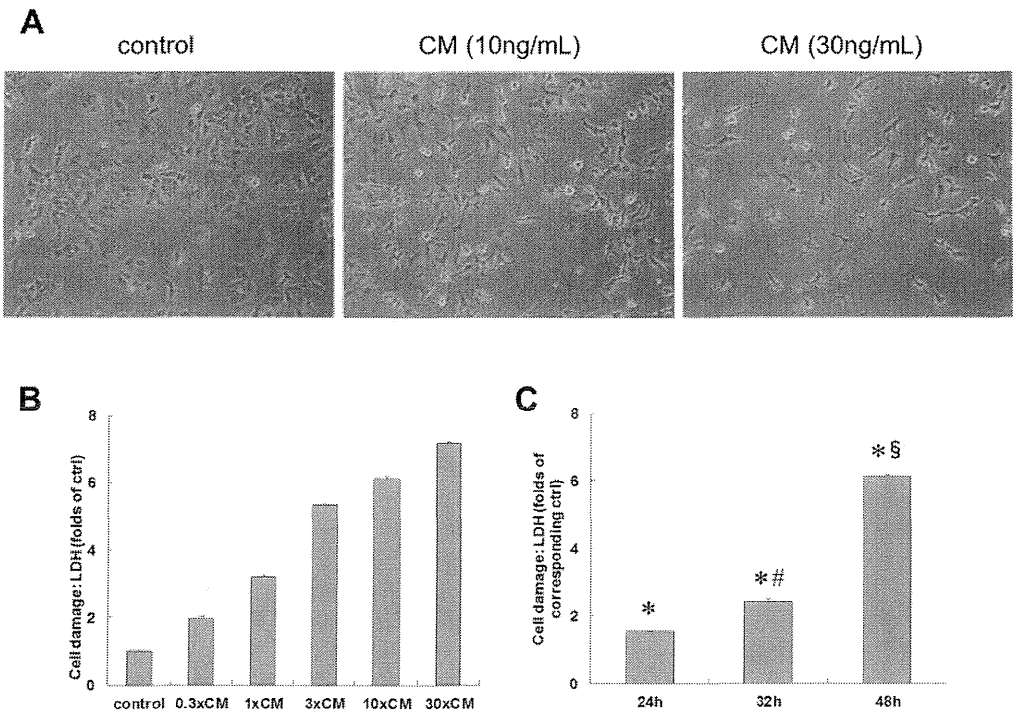

Figure 1. Cytomix induced cell death in A549 cells in a dose-dependent manner. (A) Light microscopic images of A549 cells stimulated with cytomix (CM: a mixture of IL-1β/TNF-α/IFN-γ) for 48 h. Dose dependent decrease in cell number and changes in morphology were observed. The original magnification of the images was 100×. **(B)** A549 cells were stimulated with cytomix at various concentrations. 1× CM stands for 1 ng/mL each of IL-1β, TNF-α, and IFN-γ. Cell damage was evaluated by monitoring the concentration of LDH in culture medium at 48 hours after cytomix challenge. Cytomix induced cell damage in a dose dependent manner in A549 cells. **(C)** A549 cells were stimulated with 10× CM. Cell damage was evaluated by LDH measurement at the indicated times after cytomix challenge. The cytotoxicity induced by cytomix became remarkable 48 h after cytomix challenge. Control cells were treated with the corresponding vehicle alone. Bar graph shows means ± S.E.M. $^{*}p < 0.01$ *vs.* the corresponding control, $^{\#}p < 0.01$ *vs.* 24 h, $^{\S}p < 0.01$ *vs.* 32 h.

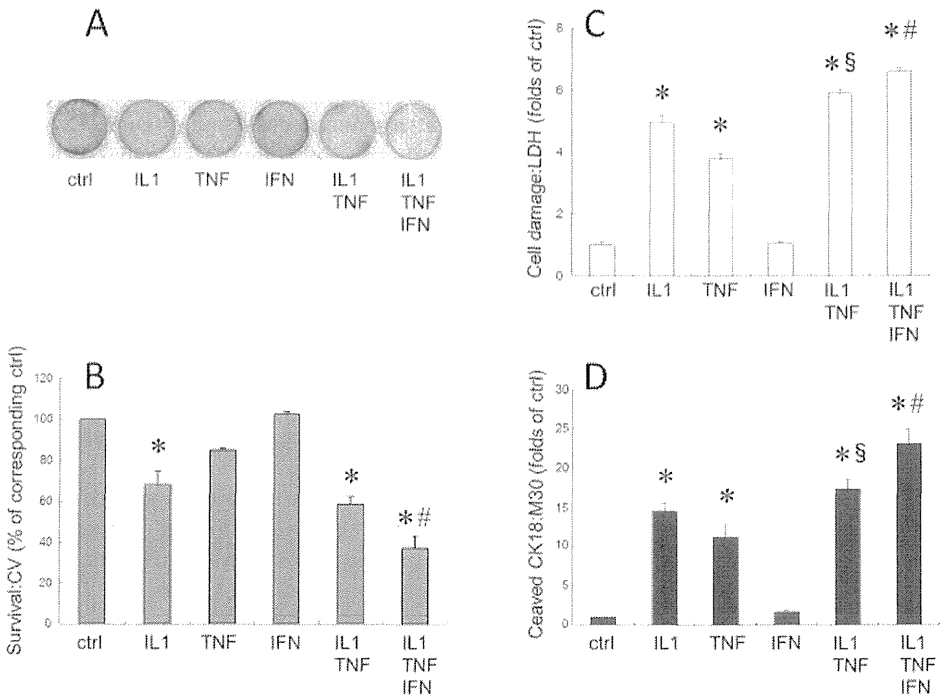

Figure 2. Mixture of proinflammatory cytokines exerted synergistic cytotoxicity in A549 cells. A549 cells were stimulated with proinflammatory cytokines, alone or in combination as indicated, for 48 h. The concentration of each cytokine was 10 ng/ml. The combination of IL-1β/TNF-α/IFN-γ was the most potent in terms of cytotoxicity. Bar graph shows means ± S.E.M. Control (ctrl) cells were treated with the corresponding vehicle alone. **(A)** Photographs showing crystal violet staining of residual cells in culture plates. **(B)** Quantitative analysis of crystal violet (CV) staining was performed as described in "Materials and Methods". $^{*}p < 0.05$ *vs.* ctrl, $^{\#}p < 0.05$ *vs.* IL1/TNF. **(C)** Cell damage was evaluated by monitoring the concentration of LDH in culture medium. $^{*}p < 0.01$ *vs.* control, $^{\S}p < 0.01$ *vs.* IL1, $^{\#}p < 0.05$ *vs.* IL1/TNF. **(D)** Caspase activation was estimated by the concentration of cleaved cytokeratin 18 in culture medium using an M30 cytodeath ELISA kit. $^{*}p < 0.01$ *vs.* control, $^{\S}p < 0.01$ *vs.* IL1, $^{\#}p < 0.05$ *vs.* IL1/TNF.

is thought to reflect the extent of apoptotic cell death, as explained in the "Materials and Methods". Similar to LDH (Figure 2C), the amount of cleaved cytokeratin 18 was increased significantly by IL-1β or TNF-α but not by IFN-γ alone (Figure 2D). In addition, cytomix showed the most prominent increase in level of cleaved cytokeratin 18.

In addition to IFN-γ, to explore a more appropriate combination of inflammatory mediators, cytotoxicity of other inflammatory mediators, such as Fas ligand, IL-6, or high-mobility group box 1 (HMGB1), was also investigated because these mediators have been reported to play significant roles in sepsis (*14,21,23*). With contrast to IFN-γ, however, Fas ligand, IL-6, or HMGB1 failed to show cytotoxicity in A549 cells, either alone or in combination with IL-1β/TNFγ, up to 100 ng/mL (Figure S1) (*http://www.biosciencetrends.com/getabstract.php?id=532*).

3.2. *Pharmacological attenuation of cytomix-induced cytotoxicity in A549 cells*

Next, to search for cytoprotective agents that can suppress the cytotoxicity induced by cytomix, various agents with antiinflammatory or antioxidative properties were extensively screened using LDH measurements. Preliminary experiments revealed that treatment with glucocorticoid (dexamethasone), tetracycline-derived antiinflammatory antibiotics (minocycline or doxycycline), angiotensin II receptor blockers (losartan or telmisartan), or antioxidants (dimethyl sulfoxide, catalase) attenuated cytomix-induced cytotoxicity in a dose dependent manner (data not shown and Table S1 (*http://www.biosciencetrends.com/getabstract.php?id=532*)). On the other hand, pharmacological agents, which failed to attenuate cytokine-induced cytotoxicity in A549 cells, are listed in Table S2 (*http://www.biosciencetrends.com/getabstract.php?id=532*).

Dexamethasone is one of the most widely used drugs for various inflammatory diseases. For ALI, it has been repeatedly reappraised (*24,25*) although its clinical validity has not been established. Dexamethasone improved cell survival after cytomix stimulation in A549 cells (Figure 3A). Dexamethasone also markedly attenuated LDH leakage (Figure 3B) and cleavage of cytokeratin 18 (Figure 3C) induced by cytomix stimulation.

Tetracycline-derived antibiotics, such as minocycline

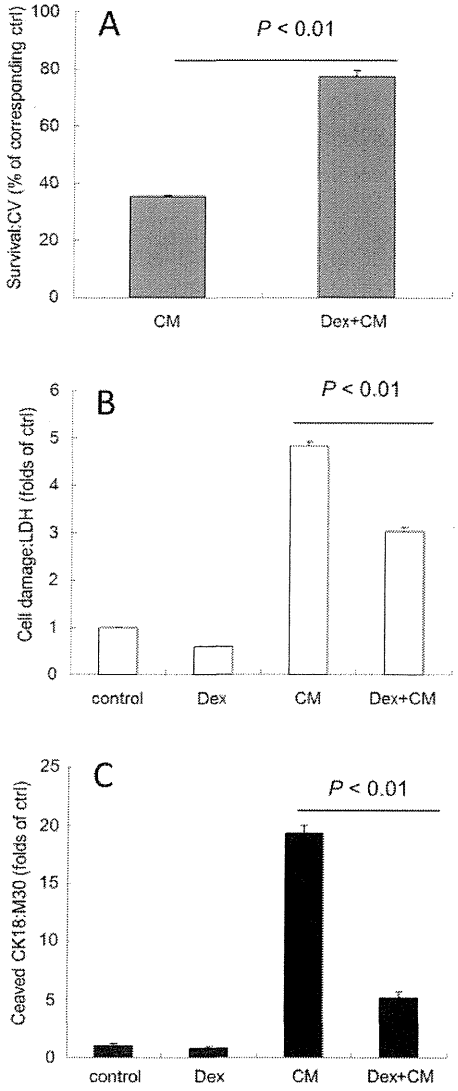

Figure 3. Dexamethasone attenuated cytomix-induced cytotoxicity in A549 cells. A549 was pretreated with dexamethasone (Dex: 1 μM) 1 h before cytomix (CM: a mixture of IL-1β/TNF-α/IFN-γ) stimulation. Forty eight hours after cytomix stimulation, cytotoxicity was evaluated as described in Materials and Methods. Control cells were treated with the corresponding vehicle alone. Bar graph shows means ± S.E.M. **(A)** Dexamethasone significantly recovered cell number in A549 cells stimulated with cytomix in crystal violet staining. **(B** and **C)** LDH and cleaved cytokeratin 18 in culture medium were also determined. Dexamethasone significantly decreased LDH **(B)** and cleaved cytokeratin 18 levels **(C)** in A549 cells stimulated with cytomix.

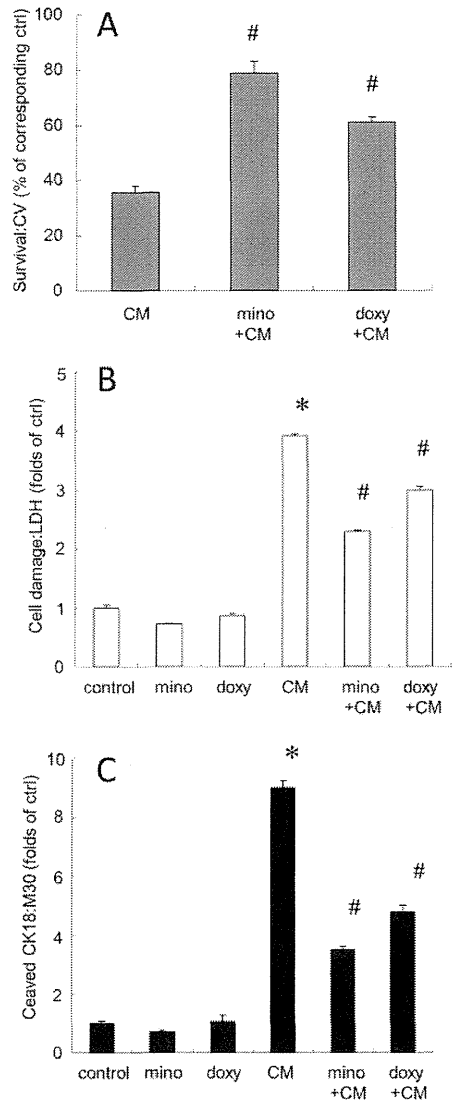

Figure 4. Tetracycline-derived antibiotics (minocycline and doxycycline) attenuated cytomix-induced cytotoxicity in A549 cells. A549 was pretreated with minocycline (mino: 100 μg/mL) or doxycyclie (doxy: 100 μg/mL) 1 h before cytomix (CM: a mixture of IL-1β/TNF-α/IFN-γ) stimulation. Forty eight hours after cytomix stimulation, cytotoxicity was evaluated as described in Materials and Methods. Control (ctrl) cells were treated with the corresponding vehicle alone. Bar graph shows means ± S.E.M. * $p < 0.01$ *vs.* control; # $p < 0.01$ *vs.* CM. **(A)** Minocycline or doxycycline significantly recovered cell number in A549 cells stimulated with cytomix in crystal violet staining. **(B** and **C)** LDH and cleaved cytokeratin 18 in culture medium were also determined. Minocycline or doxycycline significantly decreased LDH **(B)** and cleaved cytokeratin 18 levels **(C)** in A549 cells stimulated with cytomix.

or doxycycline, are known to have pleiotropic effects other than inhibiting growth of microorganisms, including antiinflammatory and cytoprotective properties (*17,26,27*). Minocycline or doxycycline was shown to attenuate the cytotoxicity induced by cytomix in A549 cells similar to dexamethasone (Figure 4) .

Angiotensin II receptor blockade has been shown to confer cytoprotection in cardiovascular tissues subjected to inflammation or ischemia/reperfusion injury (*28,29*). Some reports have argued that it is also a promising candidate for alleviating the pathophysiology of ALI (*30,31*). Losartan, the first angiotensin II receptor blocker (ARB) clinically applied, improved cell survival after cytomix stimulation in A549 cells (Figure 5A). In addition, it attenuated LDH leakage and cleavage of cytokeratin 18 induced by cytomix stimulation

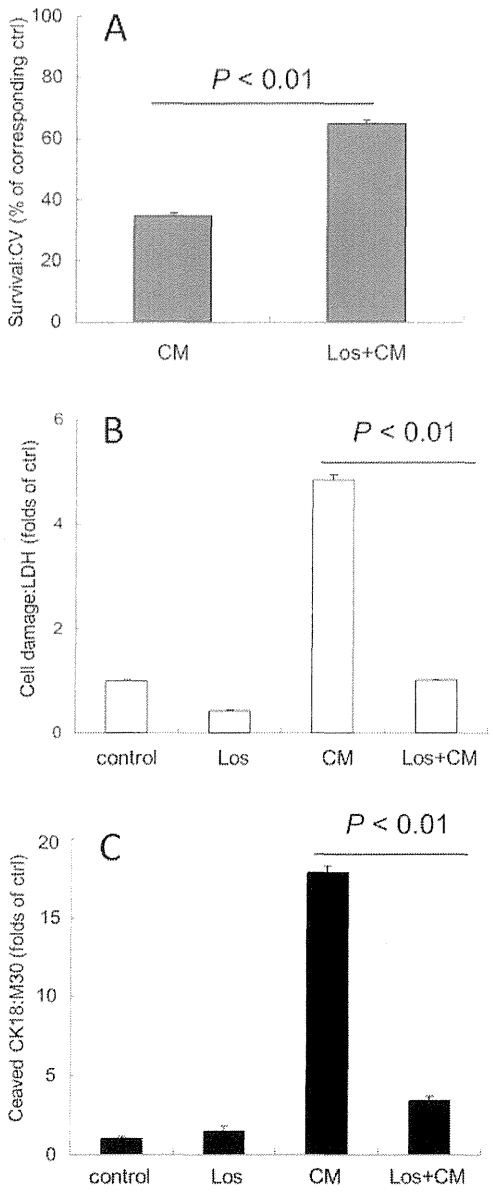

Figure 5. Losartan attenuated cytomix-induced cytotoxicity in A549 cells. A549 was pretreated with losartan (Los: 0.5 mM) 1 h before cytomix (CM: a mixture of IL-1β/TNF-α/IFN-γ) stimulation. Forty eight hours after cytomix stimulation, cytotoxicity was evaluated as described in "Materials and Methods". Control cells were treated with the corresponding vehicle alone. Bar graph shows means ± S.E.M. **(A)** Losartan significantly recovered cell number in A549 cells stimulated with cytomix in crystal violet staining. **(B** and **C)** LDH and cleaved cytokeratin 18 in culture medium were also determined. Losartan significantly decreased LDH **(B)** and cleaved cytokeratin 18 levels **(C)** in A549 cells stimulated with cytomix.

(Figures 5B and 5C). Telmisartan, another established ARB, showed similar cytoprotective effects in cytomix-stimulated A549 cells (data not shown).

Oxidative stress is potentially cytotoxic and has been implicated in the mechanisms of various diseases, including acute disease such as systemic inflammation or ischemia-reperfusion injury (*32,33*). There are a number of antioxidants with respective spectrum for neutralizing reactive oxygen species. DMSO, an important polar aprotic solvent, has antioxidant properties such as reducing lipid peroxidation (*34*). Catalase is a common enzyme found in nearly all living organisms that are exposed to oxygen, where it catalyzes the decomposition of hydrogen peroxide to water and oxygen (*35*). These antioxidants attenuated the cytotoxicity induced by cytomix in A549 cells, in terms of cell survival, cell damage, or cleavage of cytokeratin 18 (Figure 6).

3.3. *Dexamethasone or losartan still exerted cytoprotection with delayed treatment after challenge of cytomix in A549 cells*

Cytoprotective effects of dexamethasone or losartan were tested as therapeutic agents, meaning that drug administration began after cytomix challenge in A549 cells. Dexamethasone (Figures 7A and 7B) or losartan (Figures 7C and 7D) still conferred cytoprotection significantly with delayed administration up to 12 hours after cytomix challenge, although the degree of cytoprotection decreased compared to pretreatment.

4. Discussion

The main findings of the present study can be summarized as follows:

1. A mixture of proinflammatory cytokines (IL-1β/TNF-α/IFN-γ) exerted synergistic cytotoxic effects in the human alveolar epithelial cell line A549.

2. Cytokine-induced cytotoxicity was mediated at least partially by the caspase-dependent apoptotic signaling pathway.

3. Antiinflammatory agents, such as glucocorticoid (dexamethasone), tetracycline-derived antibiotics (minocycline, doxycycline), angiotensin II receptor blockers (losartan, telmisartan), or antioxidants (DMSO, catalase) showed prominent cytoprotective effects against the cytotoxicity induced by proinflammatory cytokines.

4. Dexamethasone or losartan still exerted cytoprotection following late treatment after challenge of cytomix in A549 cells.

IL-1β and TNF-α are postulated to be the two main proinflammatory cytokines involved in systemic inflammation (*7,11*). Either of these cytokines alone can induce clinical manifestations, such as hypotension, high fever, chills, and organ dysfunction, representative of sepsis (*22*). In the present study, these cytokines showed cytotoxicity in A549 cells. Although IFN-γ has not yet been regarded as essential in pathophysiology of sepsis like IL-1β or TNF-α, this study clearly showed that it enhanced the cytotoxicity of IL-1β and TNF-α. In fact, the importance of IFN-γ in the native

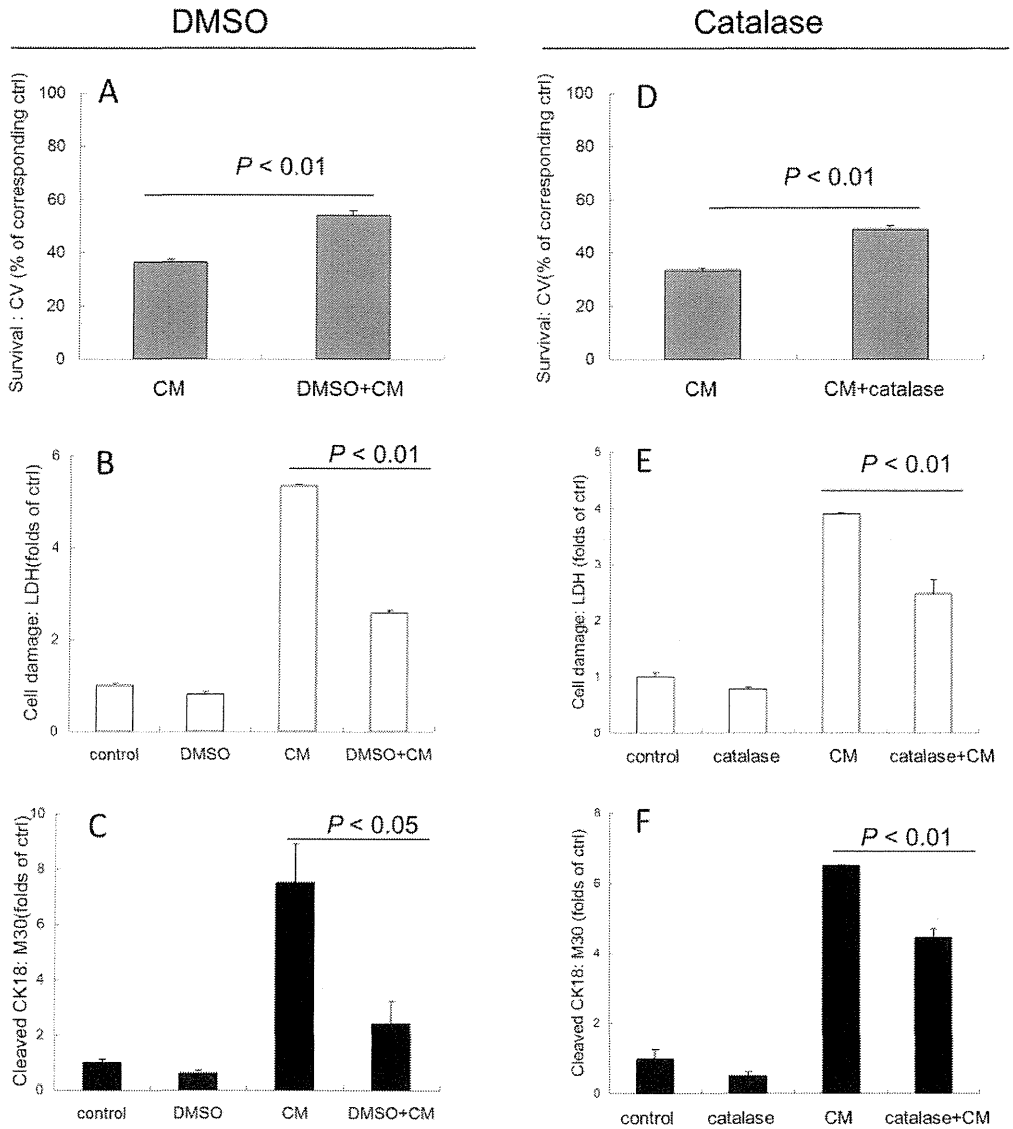

Figure 6. Antioxidants (DMSO or catalase) attenuated cytomix-induced cytotoxicity in A549 cells. A549 was pretreated with dimethyl sulfoxide (1% DMSO, **A-C**) or catalase conjugtated to polyethylene glycol (1,000 unit/mL, **D-F**) 1 h before cytomix (CM: a mixture of IL-1β/TNF-α/IFN-γ) stimulation. Forty eight hours after cytomix stimulation, cytotoxity was evaluated as described in "Materials and Methods". Control (ctrl) cells were treated with the corresponding vehicle alone. Bar graph shows means ± S.E.M. DMSO **(A)** or catalase **(D)** significantly recovered cell number in A549 cells stimulated with cytomix in crystal violet staining. LDH and cleaved cytokeratin 18 in culture medium were also determined. DMSO **(B and C)** or catalse **(E and F)** significantly decreased LDH and cleaved cytokeratin 18 levels in A549 cells stimulated with cytomix.

immune system has recently attracted a great deal of attention (*36*). For example, IFN-γ promotes innate immune response by activating macrophage, which plays major roles in eliminating infectious pathogens. IFN-γ enhances immune cell responsiveness to other inflammatory stimuli, such as toll-like receptor ligands and TNF. This phenomenon, termed as "priming", greatly augments toll-like receptor-induced expression of inflammatory mediators and immune effectors including multiple cytokines and chemokines, and profoundly affects biological outcomes of inflammation.

In a murine model of sepsis induced by cecal ligation and puncture (CLP), late administration of anti-IFN-γ antibody enhanced survival (*37*). In fact, high levels of IFN-γ has been demonstrated in some populations with clinical systemic inflammation, especially in virus-associated ALI such as SARS (severe acute respiratory syndrome) (*8,10*). Multiple inflammatory mediators have been proved in the bloodstream and bronchoalveolar lavage fluid of patients with septic ALI (*10-13*). The observation that a mediator such as IFN-γ, which has minimal direct toxicity against

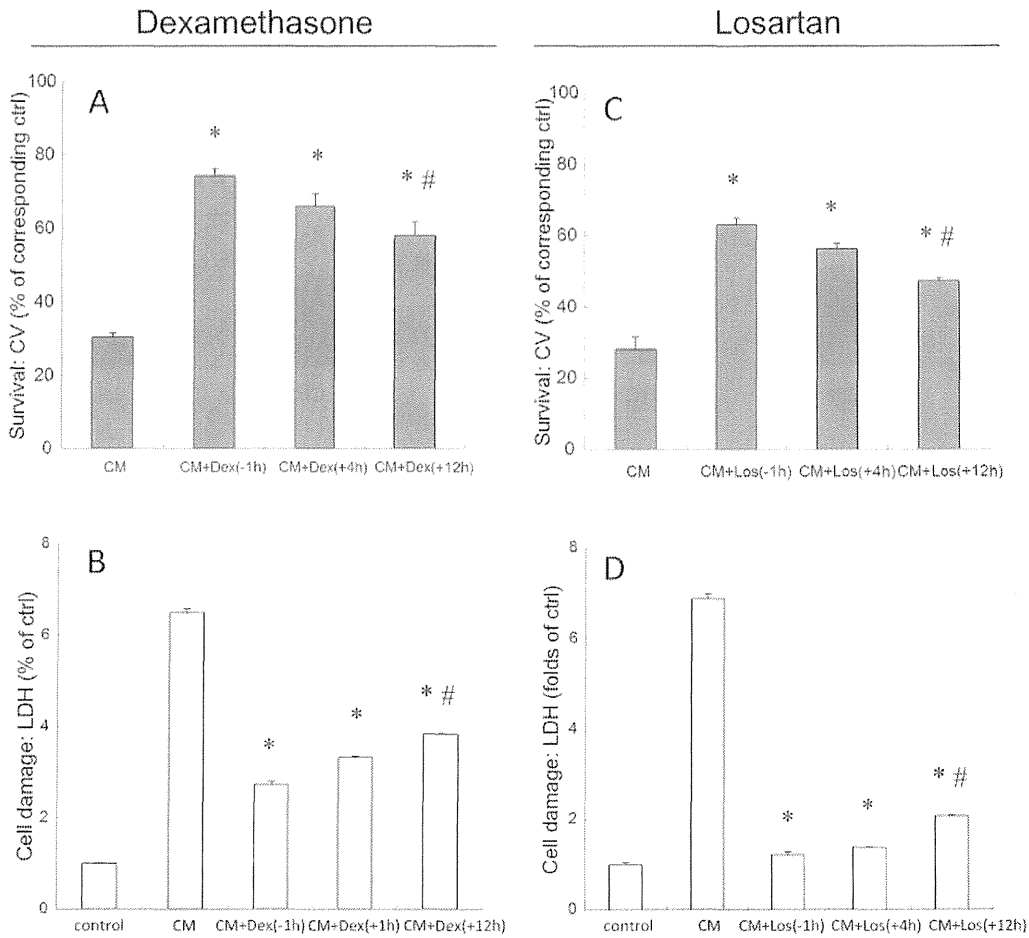

Figure 7. Dexamethasone or losartan still exerted cytoprotection with delayed treatment after cytomix challenge in A549 cells. A549 was stimulated with cytomix (CM: a mixture of IL-1β/TNF-α/IFN-γ). Co-treatement of either dexamethasone (1 μM or losartan (0.5 mM) was initiated 1 h before (−1 h), 4 h after (+4 h), or 12 h after (+12 h) cytomix stimulation. Sixty hours after cytomix stimulation, cytotoxicity was evaluated by crystal violet staining and LDH measurement. Dexamethasone **(A** and **B)** or losartan **(C** and **D)** still conferred cytoprotection significantly with delayed treatment up to 12 h after cytomix challenge, although the degree of cytoprotection decreased significantly compared to pretreatment (−1 h). Control (ctrl) cells were treated with the corresponding vehicle alone. Bar graph shows means ± S.E.M. $^{*}p < 0.01$ *vs.* CM; $^{\#}p < 0.01$ *vs.* pretreatment (−1 h).

parenchymal cells, can exert synergistic cytotoxicity in combination with other mediators implies the complex pathophysiology of sepsis and suggests one reason for the failure of antiinflammatory strategies targeting a single mediator such as IL-1β or TNF-α (*38*).

Neutrophil recruitment and epithelial injury play pivotal roles in the development of ALI (*5-7,21*). A number of inflammatory mediators, such as proinflammatory cytokines, lipid mediators, complements, reactive oxygen species or neutrophil-derived ptoteases such as elastase (*39*), are postulated to be responsible for loss of epithelial integrity. However, there is little doubt that proinflammatory cytokines make a substantial contribution in initiating the pathological process of septic ALI. Thus, elucidation of the direct link between proinflammatory cytokines and epithelial injury, focusing on molecular mechanisms, is indispensable to understand the progression of septic ALI. The present study confirmed that human alveolar epithelial cells were damaged after challenge by proinflammatory cytokines. Cell death evoked by cytokine challenge was remarkable, and the increase in level of cleaved cytokeratin 18 strongly suggested the substantial involvement of caspase-dependent apoptosis. These results are compatible with other reports arguing that apoptosis pathways are activated in septic ALI experimentally or clinically (*5-7,11,40,41*).

As it has been established that hyperinflammatory status is the major pathophysiology of septic ALI, modifying inflammation should be highlighted as one of the central strategies for alleviating septic ALI. Although protective ventilatory strategies have been shown to lessen mortality in ALI patients (*4*), the way of directly downregulating inflammation itself has not been fully examined. In addition, there is increasing evidence that oxidative stress as well as nitrosative

stress prevails at sites of inflammation as adaptive responses of the host, such as antimicrobial strategies or stress-evoked signal transduction (*32,33*). As excessive oxidative stress in turn causes tissue damage of host cells, alleviation of oxidative stress can be a promising alternative to controlling inflammation-associated injury in septic ALI (*42,43*). In the present study, we screened agents with antiinflammatory or antioxidative properties for cytoprotective effects in the *in vitro* model mimicking alveolar hyperinflammation. We have demonstrated that antiinflammatory agents dexamethasone, tetracycline-derived antibiotics, or ARBs attenuated cytokine-induced cytotoxicity including caspase activation in A549 cells. In addition, antioxidants such as DMSO or catalase similarly attenuated cytokine-induced cytotoxicity. These agents have been referred to as cytoprotective in inflammation-associated conditions (*24-35*), although clinical validity has not been fully defined, especially in septic ALI. Further investigations are underway to clarify the mechanism of pharmacological attenuation of cytokine-induced cytotoxicity. It is widely accepted that inflammatory stimuli activate NF-kappaB pathway and MAP kinase pathway (*44*). Simultaneously, oxidative stress contributes to epithelial injury because catalase was effective in attenuating inflammation-associated cell death in the present results. Thus, we are now focusing on NF-kappaB pathways, MAP kinase pathways and sources of oxidative stress (such as mitochondria, NADPH oxidase, xanthine oxidase, inducible nitric oxide synthase, or arachidonic acid cascade), as cytotoxic signal pathways evoked by inflammatory stimuli (Figure 8).

The present study has some limitations. First, A549 is a cancer cell line and its intrinsic cell death pathways may differ from those of physiological human alveolar epithelial cells. Second, cytotoxic mediators employed here were IL-1β/TNF-α/IFN-γ and it is not clear whether this combination is optimal in simulating *in vivo* hyperinflammatory status. Third, the methods used to detect cell death in our experiments were limited. For example, the apoptotic component was estimated based on the level of cleaved cytokeratin 18 and was not confirmed directly by morphological evidence of apoptosis.

However, it is important to check the signaling pathway using human cells as well as using *in vivo* animal models. It is practically impossible to include all of inflammatory mediators as stimulants. The combination of IL-1β/TNF-α/IFN-γ has often been adopted to set up hyperinflammation *in vitro* and accepted in many medical journals (*15-17,45-48*). In the present study it exerted sufficient cytotoxicity with clinical relevance as discussed earlier. It is reported that in clinical septic patients, numerous cytokines, irrespective pro-, or anti-inflammatory, appear in an overlapping manner as long as inflammatory process

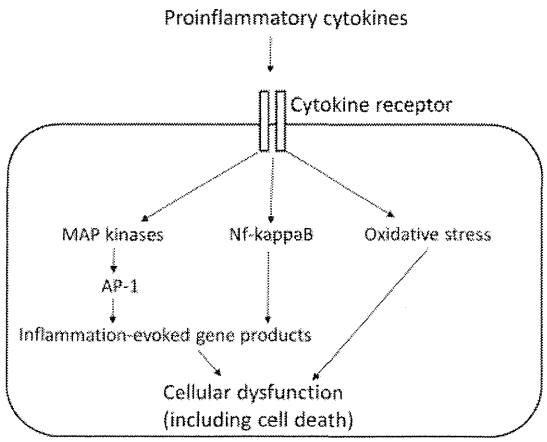

Figure 8. Proposed signaling pathways through which proinflammatory cytokines induce cytotoxicity in alveolar epithelial cells. Putative intracellular signaling components responsible for proinflammatory cytokine-induced cellular dysfunction are shown. It is postulated that cytoprotective agents will interfere in somewhere in the above-mentioned signaling pathways (see "Discussion"). MAP kinase: mitogen activated protein kinase; AP-1: activating protein-1.

continues (*49*). Thus, we postulate that IL-1β/TNF-α/IFN-γ is a minimum and appropriate mixture to simulate the status of clinical cytokine storm in *in vitro* system. Lastly, direct confirmation of apoptosis was not the main objective of this study. Apoptosis is now regarded as just one form of cell death patterns in the recent framework explaining the physiological cell death mechanism (*6*). Thus, evaluation of overall cytotoxicity is more important when differential demonstration of other cell death patterns, such as autophagy, necroptosis, or caspase-independent other programmed cell death, has not been well established yet.

In conclusion, inflammatory cytokines showed synergistic cytotoxic effects on A549 cells. Caspase-dependent apoptosis was speculated to be one mechanism responsible for the cytokine-induced cytotoxicity. Agents with antiinflammatory or antioxidative properties such as glucocorticoid, tetracycline-derived antibiotics, angiotensin II receptor blockers, or antioxidants showed substantial effect in attenuating cytokine-induced cytotoxicity. Further investigations to clarify the mechanisms of their beneficial effects will contribute to exploring new treatment options for ALI.

Acknowledgements

We thank Dr. Fumito Ichinose (Boston, MA, USA) and Dr. Masaomi Nangaku (Tokyo, Japan) for the critical reading of the paper and insightful suggestions. This work was supported in part by grants from the Ministry of Education, Culture, Sports, Science and Technology of Japan (No. 21592304 to K.C.).